PONTIFICIA UNIVERSIDAD CATÓLICA DEL PERÚ

ESCUELA DE POSGRADO

NEUTRINO TRIDENT PRODUCTION REVISITED FOR DUNE-LIKE AND MINERVA-LIKE SCENARIOS

Artículo para optar por el grado de Magíster en Física

Autor

Sebastián de Jesús Sánchez Falero

Asesor

Dr. Alberto Martín Gago Medina

Jurado

Dr. Joel Jones Pérez

Dr. José Luis Bazo Alba

Lima, Perú - 2017

Agradecimientos

Gracias a la vida.

Resumen

Revisamos sistemáticamente el proceso de producción de di-muones via la dispersión de neutrinos en el campo Coulombiano del núcleo, conocido como producción tridente de neutrinos. A pesar de que este proceso tiene una sección de choque pequeña comparada con el proceso de dispersión neutrino-núcleo via corriente cargada inclusiva en el Modelo Estándar, se caracteriza por una señal experimental muy clara. El par de muones cargados opuestamente es caracterizado investigando sus distribuciones cinemáticas. Para esto, hemos implementado una simulación detallada del proceso de producción tridente de neutrinos en el generador de eventos Montecarlo GENIE; y analizamos y simulamos los backgrounds relevantes. También exploramos métodos de Análisis Multivariado para mejorar la selección de la señal en el contexto de detectores tipo MINERνA y DUNE como representantes de experimentos de neutrinos de aceleradores presentes y venideros.

Abstract

We systematically review the di-muon production via neutrino scattering off the Coloumb field of nuclei, referred to as neutrino trident production. While this process has a small cross section compared to the SM charged-current inclusive neutrino nucleus channel, it features a very clear experimental signature. The oppositely charged muons are characterized by investigating their kinematical distributions. For this, we have implemented a very detailed simulation of neutrino trident production in the GENIE MC and make an analysis and simulation of relevant backgrounds. We further explore Multivariate Analysis methods to enhance signal selection in the context of a MINERνA-like and DUNE-like detectors as representative of current and forthcoming accelerator-based neutrino experiments.

Neutrino Trident Production revisited for DUNE-like and MINERvA-like scenarios

S. Sánchez Falero,* J. Becerra,† E. Endress,‡ and A. M. Gago§
Sección Física, Departamento de Ciencias, Pontificia Universidad Católica del Perú, Apartado 1761, Lima, Perú
(Dated: May 16, 2017)

We systematically review the di-muon production via neutrino scattering off the Coloumb field of nuclei, referred to as neutrino trident production. While this process has a small cross section compared to the SM charged-current inclusive neutrino nucleus channel, it features a very clear experimental signature. The oppositely charged muons are characterized by investigating their kinematical distributions. For this, we have implemented a very detailed simulation of neutrino trident production in the GENIE MC and make an analysis and simulation of relevant backgrounds. We further explore Multivariate Analysis methods to enhance signal selection in the context of a MINERνA-like and DUNE-like detectors as representative of current and forthcoming accelerator-based neutrino experiments.

PACS numbers: 13.15.+g, 13.40.Gp

I. INTRODUCTION

In the Standard Model (SM), there exists a reaction in which a neutrino induces the production of lepton triplets through the scattering off the Couloumb field of a nucleus. This process is called neutrino trident production and can occur via charged current (CC) and neutral current (NC) channels (fig. 1). In fact, it has been extensively studied since several decades ago [1–6], being one of the few process where the weak-interaction theory of the SM can be directly tested. The latter is due to the interference between the charged and neutral current contributions that are taking place in the reaction.

The observation of neutrino trident events is very challenging since it exhibits extremely small cross sections, this is $\sim 10^{-5}$ times the inclusive ν_μ nucleon CC process for incoming neutrino energies up to $O(100$ GeV). First evidences of trident events were given by CHARM[7], allowing only constraints over the weak diagonal coupling constant. Later, the CHARM II [8] experiment, using a neutrino beam with $\langle E_\nu \rangle \sim 160$ GeV and an iron target was able to report the first cross section measurement, which resulted to be consistent with SM. The CCFR [9] experiment, using a neutrino beam with $\langle E_\nu \rangle \sim 20$ GeV and a glass target, was finally able to report a cross section conclusively confirming the weak interference and ruling out pure V-A hypothesis at 99% CL. Later, the NUTEV [10] experiment also reported an excess of low hadronic vertex energy events consistent with the trident expectation from SM.

$$\begin{aligned} \sigma_{\text{CHARM-II}}/\sigma_{\text{SM}} &= 1.58 \pm 0.57, \\ \sigma_{\text{CCFR}}/\sigma_{\text{SM}} &= 0.82 \pm 0.28 \end{aligned}$$

Recently, interest in neutrino trident production has re-emerged in the context of studying New Physics (NP). As such it can, e.g., be used as a probe for hypothetical new NC among leptons due to a gauge symmetry in the difference between the muon and tau flavor number, $L_\mu - L_\tau$ [11]; the vector boson Z' arising from this interaction would modify the SM expectancy by a sizable amount due to its interference with the contributions from SM weak bosons. Nevertheless, in order to be successful in any search of New Physics through the trident process, it is of utmost importance to be able to disentangle the scarce number of signal events from the background. For instance, if we particularly focus on the trident events that produce di-muons, we have to deal with various SM background contributions. The di-muon production can happen in Deep Inelastic Scattering (DIS), resonance excitations, charm production, and charged current inclusive pion production. Additionally, for the last one, the pion itself or the anti-muon coming from its decay, jointly with the muon originating from the first interaction vertex, can be misreconstructed as a di-muon pair.

*Electronic address: sebastian.sanchez@pucp.edu.pe
†Electronic address: josea.becerra@pucp.pe
‡Electronic address: eric.endress@gmx.de
§Electronic address: agago@pucp.edu.pe

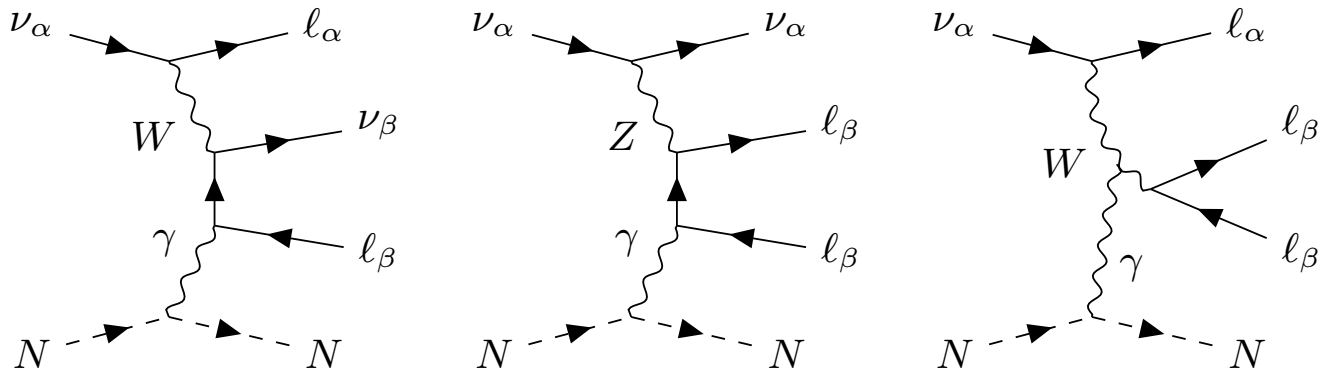

FIG. 1: Tree-level Feynman diagrams for neutrino trident production, for $\alpha, \beta = e, \mu, \tau$. Corresponding to the first and second, there exist additional diagrams where the photon couples to the other muon. The last diagram is largely suppressed due to the presence of two W propagators.

The aim of the present work is to perform an optimization analysis for the signature of trident events in different experimental frameworks. We have chosen to study the process with a di-muon pair in the final state because it is by far the clearest experimental channel. There has been recent work [12] that analyzes the possibility of observing trident events using electrons in the final state, but its detection capability relies on having a liquid argon detector.

We have reviewed different experimental frameworks, considering for neutrino fluxes those provided by the NuMI[13] or LBNF[14] beamlines. The former is currently in the Medium Energy mode ($\langle E_\nu \rangle \sim 6$ GeV) and is expected to deliver $\sim 4 \times 10^{21}$ POTs over the course of two years of operation [15]. The LBNF flux is expected to provide $\sim 1.5 \times 10^{21}$ POTs per year, with $\langle E_\nu \rangle \sim 3$ GeV [16]. We have considered carbon and argon as possible detector materials. The carbon would mimic an experiment like MINERvA [17] or a fine grained tracker option for the DUNE [18] Near Detector (ND); while the argon would represent, e.g., the liquid argon option for DUNE ND.

In order to achieve a realistic analysis, we have implemented a detailed simulation of the trident process [19] in the state of the art GENIE Neutrino MC Generator [20]. This is a powerful tool for the analysis since we have at our disposal all the kinematical distributions of the process. In fact, our simulation could even be used within the context of the Montecarlo event generator of an experiment for future trident searches. We have also reanalysed the background processes using up-to-date models in GENIE and giving emphasis on pion production channels. Relevant backgrounds have furthermore been propagated in a non-oversimplified detector geometry within the GEANT4[21] framework. For refining the signal selection we have applied Multi Variate Analysis (MVA) techniques on the trident kinematical quantities, on top of the usual topological cuts.

This paper is structured as follows: we begin by reviewing the theory of neutrino trident interactions II and cross section calculation in section III. Then, in section IV we discuss the signal, backgrounds and the simulation tools implemented and used. Following, section V is devoted to describing the analysis framework and multivariate techniques we applied for the signal separation in definite experimental contexts. We finally discuss our results (section VI) and conclude (VII) commenting on the possibilities for prospective NP searches in light of our findings.

II. THEORETICAL ASPECTS

In the SM, reaction trident production occurs at tree level through a total of five diagrams (fig. 1). A direct coupling of the photon to the W is largely suppressed due to the mass of the weak boson in the resulting two propagators. The interaction with the target is purely electromagnetic, rendering trident production one of the few possible processes to study lepton interactions without hadronic physics obscuring the picture in the form of weak form factors [4]. Due to the smallness of muon mass m, it has a very low threshold $E_\nu^{\rm thr} = 3m + 2m^2/M_{Target}$ and it is not kinematically limited as other purely leptonic processes like, e.g. muon decay.

Current typical accelerator neutrino beams comprise energy regimes sufficiently below the Glashow resonance, where neutrino trident production can be studied through a local four-point effective interaction and single-photon exchange with a nuclear target. Similar to the case of the neutrino-electron scattering, a Fierz transformation can be performed to relate the CC and NC amplitudes, so that the resulting amplitude has the V-A form, but with different values of the vector- and axial-vector-coupling strengths C_V and C_A. The calculation thus starts from the effective Lagrangian [22]

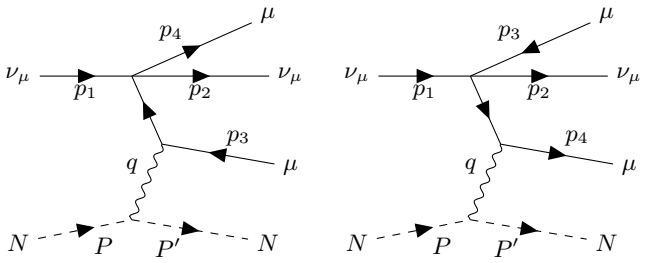

FIG. 2: 4 point effective diagrams used in calculations and momenta label convention

$$\mathcal{L} = \frac{G_F^2}{\sqrt{2}} \bar{\mu}\gamma_\alpha \left(C_V - \gamma_5 C_A\right) \mu \bar{\nu}\gamma^\alpha \left(1 - \gamma_5\right) \nu \tag{1}$$

Despite its simplicity, it already constitutes an admixture of charged and neutral currents. The Feynman diagrams stemming from this lagrangian are those shown in figure 2. Furthermore, under the single photon exchange assumption, the total invariant amplitude $|\mathcal{M}^2|$ for the trident process arising from lagrangian 1 factorizes in a leptonic and an hadronic part, thus allowing to express the total cross section σ_{SM} under the general structure [6]

$$\sigma^{SM} = C_V^2 \sigma_{C_V^2} + C_A^2 \sigma_{C_A^2} + C_V C_A \sigma_{C_V C_A} \tag{2}$$

Recall that, having the same vector and axial-vector couplings C_V and C_A, the total cross section for the antineutrino trident cross section is the same as for neutrino, $\sigma_\nu^{\text{trident}} = \sigma_{\bar{\nu}}^{\text{trident}}$.

Explicitly, the trident cross section [1] is

$$\sigma^{SM} = \frac{2Z^2\alpha^2 G_F^2}{(2\pi)^6} \frac{1}{4M_T E_1} \int \frac{d^3P'}{2E'} \, \mathcal{F}_{\mu\nu}(P,q) \, \mathcal{L}^{\mu\nu}(p_1,q) \, \frac{1}{q^4}, \tag{3}$$

where M_T is the target mass, E' the final target energy and $q = P - P'$ the momentum transfer to the nucleus. Note that this expression is exact to order $\alpha^2 G_F^2$ [1].

The leptonic contribution is contained in

$$\mathcal{L}_{\mu\nu}(p_1,q) = \int \frac{d^3p_2}{2E_2} \int \frac{d^3p_3}{2E_3} \int \frac{d^3p_4}{2E_4} \, \delta^4\left(q + p_1 - p_2 - p_3 - p_4\right) \mathcal{M}_{\mu\nu} \quad , \tag{4}$$

$$\begin{aligned} \mathcal{M}_{\mu\nu} = {} & \text{Tr}\left\langle \gamma^\lambda \left(1-\gamma_5\right) \not{p}_1 \gamma^\sigma \left(1-\gamma_5\right) \not{p}_2 \right\rangle \times \\ & \text{Tr}\left\langle \left[\gamma_\mu \frac{1}{i\not{p}_4 - i\not{q} + m} \gamma_\lambda \left(C_V - C_A\gamma_5\right) + \gamma_\lambda \left(C_V - C_A\gamma_5\right) \frac{1}{i\not{q} - i\not{p}_3 + m} \gamma_\mu \right] \times \right. \\ & \left. \left(-m - i\not{p}_3\right) \left[\gamma_\nu \frac{1}{i\not{q} - i\not{p}_3 + m} \gamma_\sigma \left(C_V - C_A\gamma_5\right) + \gamma_\sigma \left(C_V - C_A\gamma_5\right) \frac{1}{i\not{p}_4 - i\not{q} + m} \gamma_\nu \right] \left(m - i\not{p}_4\right) \right\rangle \end{aligned} \tag{5}$$

where $E_1 - E_4$ are the lepton energies and $\mathcal{M}_{\mu\nu}$ is the square of the lepton current summed over spins with the muon mass m.

Finally, the square of the matrix element of the hadronic electromagnetic current $\mathcal{F}_{\mu\nu}$ can be obtained from standard EM scattering theory off a spin-0 nuclear target [1]

$$\begin{aligned} \mathcal{F}_{\mu\nu}(P,q) &= \mathcal{F}_{\nu\mu}(P,q) \\ &= 4|F(q^2)|^2 \left(P_\mu - \frac{1}{2}q_\mu\right)\left(P_\nu - \frac{1}{2}q_\nu\right) \end{aligned} \tag{6}$$

The nuclear form factors strongly limit the high-energy dependence of the cross section for the *Coherent* processes, i.e., when the neutrino scatters off a nucleus which acts as a single entity

$$\nu_\mu + Z \to Z + \mu^+ + \mu^- + \nu_\mu, \tag{7}$$

Therefore, it is also necessary to study the *Incoherent* process

$$\nu_\mu + N \to N + \mu^+ + \mu^- + \nu_\mu, \qquad N = n, p \tag{8}$$

where the scattering occurs off individual nucleons within nuclei. Since nucleons contribute independently, this gives an incoherent contribution to be added to the coherent one.

In the Incoherent case, the cross section is limited by the nucleon form factors and therefore falls off more slowly. The hadronic electromagnetic current part can then be written as

$$\begin{aligned}\mathcal{F}_{\mu\nu}(P,q) = q^2|F_1(q^2) + 2M_T F_2(q^2)|^2 \left(\delta_{\mu\nu} - \frac{q_\mu q_\nu}{q^2}\right) + \\ \left(|F_1(q^2)|^2 + q^2|F_2(q^2)|^2\right) 4 \left(P_\mu - \frac{1}{2}q_\mu\right)\left(P_\nu - \frac{1}{2}q_\nu\right)\end{aligned} \tag{9}$$

for incoherent scattering from a spin-$\frac{1}{2}$ nucleon. For the individual nucleon form factors, the following dipole parameterizations [1] are used

$$f_{1p} = f_{2p} = f_{2n} = \frac{1}{(1 + 1.21q^2/M_p^2)^2}, \qquad f_{1n} = 0. \tag{10}$$

Since $\mathcal{F}_{\mu\nu}(P,q) = \mathcal{F}_{\nu\mu}(P,q)$, only the symmetric parts of $\mathcal{M}_{\mu\nu}$ will contribute [1, 4].

Finally a noteworthy remark: the production of a real W, i.e.

$$\nu_\mu + N \to N + W^+ + \mu^-, \tag{11}$$

which consequently decays into leptons

$$W^+ \to \mu^+ + \nu_\mu, \tag{12}$$

leads to the same final state as eq.7. However, in subsequent section we will address the issue of analogous reactions where instead of the W, a meson is produced and decays. This processes have much higher cross sections and do constitute a serious background for trident production.

III. TOTAL CROSS SECTION

To perform the phase-space integration of the four-particle final state of eq. 3, it is useful to rewrite the variables so that they are expressed in terms of scalar products of various momenta, i.e. Lorentz invariant quantities. This change of variables is outlined in CSW [1]. Although the problem of phase space integration is conceptually rather easy, in practice the calculation is computationally expensive due to the extreme peaking of the square of the matrix element in phase space resulting from the sharp fall-off of the form factor for larger momentum transfer. Suitable variable transformations [4] help to smoothen the integrand in the Coherent case and render the Monte Carlo integration substantially faster. We performed the numerical computations using the VEGAS [23] algorithm first through the Cuba library [24] and later through the GNU Scientific Library (GSL) [25] in our native trident implementation in GENIE.

A. Coherent Process

The nuclear physics in the Coherent process is largely determined by the nuclear electromagnetic form factor $F(q^2)$, defined as the Fourier transform of the nuclear charge density in the Breit frame (in which $q_0 = 0$)

$$F(q^2) = \frac{\int \rho(r) e^{i\vec{q}\cdot\vec{r}} dr^3}{\int \rho(r) dr^3} \tag{13}$$

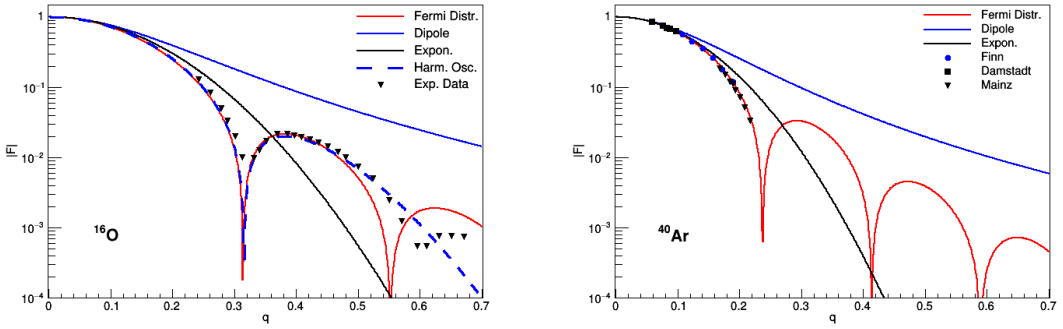

(a) O-16 (b) Ar-40

FIG. 3: Comparison of different form factor models for relevant target nuclei. Measurement references are from [26].

Standard forms used in the earlier works are the dipole and exponential fit,

$$F(q^2) = \frac{1}{\left(1 - q^2 R_0^2/20\right)^2}, \qquad F(q^2) = e^{q^2 R_0^2/10}, \tag{14}$$

respectively, with $R_0 = 1.3\ A^{1/3} \times 10^{-13}$cm.

These simple parameterizations reproduce the experimental data rather poorly as illustrated in Fig. 3 and overestimate the actual value of the cross section as can be seen in Fig. 4.

A two-parameter Fermi distribution for the charge density

$$\rho(r) = \rho_F(r) = \frac{\rho_0}{1 + e^{(r-c)/z}}, \tag{15}$$

is commonly used for a fit to experimental data. Here, c, z are parameters which are summarized for various elements in Ref. [26]. The evaluation of the Fermi form factor can then be performed numerically. In this work we use an analytic form of a symmetrized Fermi-model [27]

$$F(Q) = \frac{3\pi Qz\,(\pi Qz\coth(\pi Qz)\sin(Qc) - Qc\cos(Qc))}{Q^3\sinh(\pi Qz)(c^2 + \pi^2 z^2)c} \tag{16}$$

where $Q = \sqrt{Q^2} = \sqrt{-q^2}$. A further phenomenological model, the Harmonic-oscillator model, was also considered with the parameters taken from Ref. [26] for an oxygen target.

This parameterization displays very good agreement with data. Furthermore, beyond the first diffraction minimum, it reaches values of the order of one percent which will suppress any further contribution to the trident cross section.

In figure 4, we compare the effect of different form factors over the total trident cross section. It highlights the importance of using the measured form factor for a given target material in order to remove any remaining uncertainty from the theoretical prediction. The dipole fit tends to overestimate the cross section by as much as 200%, particularly at low energies.

Next, we examine the influence of different atomic number on the total cross section (fig. 5). Although from a higher Z will always give a higher trident cross section for a given energy, when compared to the CC cross section, the influence of Z is not so drastic. At energies lower than ~ 4 GeV, experiments having low Z may have a higher proportion of tridents. Overall, for increasing the fraction or the absolute number of trident events, both a higher E_ν and Z are beneficial.

B. Incoherent Process

Just as with common neutrino-nucleus scattering, the transitioning of trident production across energy scales can be idealized in major regimes, the Coherent being the dominant at low momentum transfer [28]. As the incoming

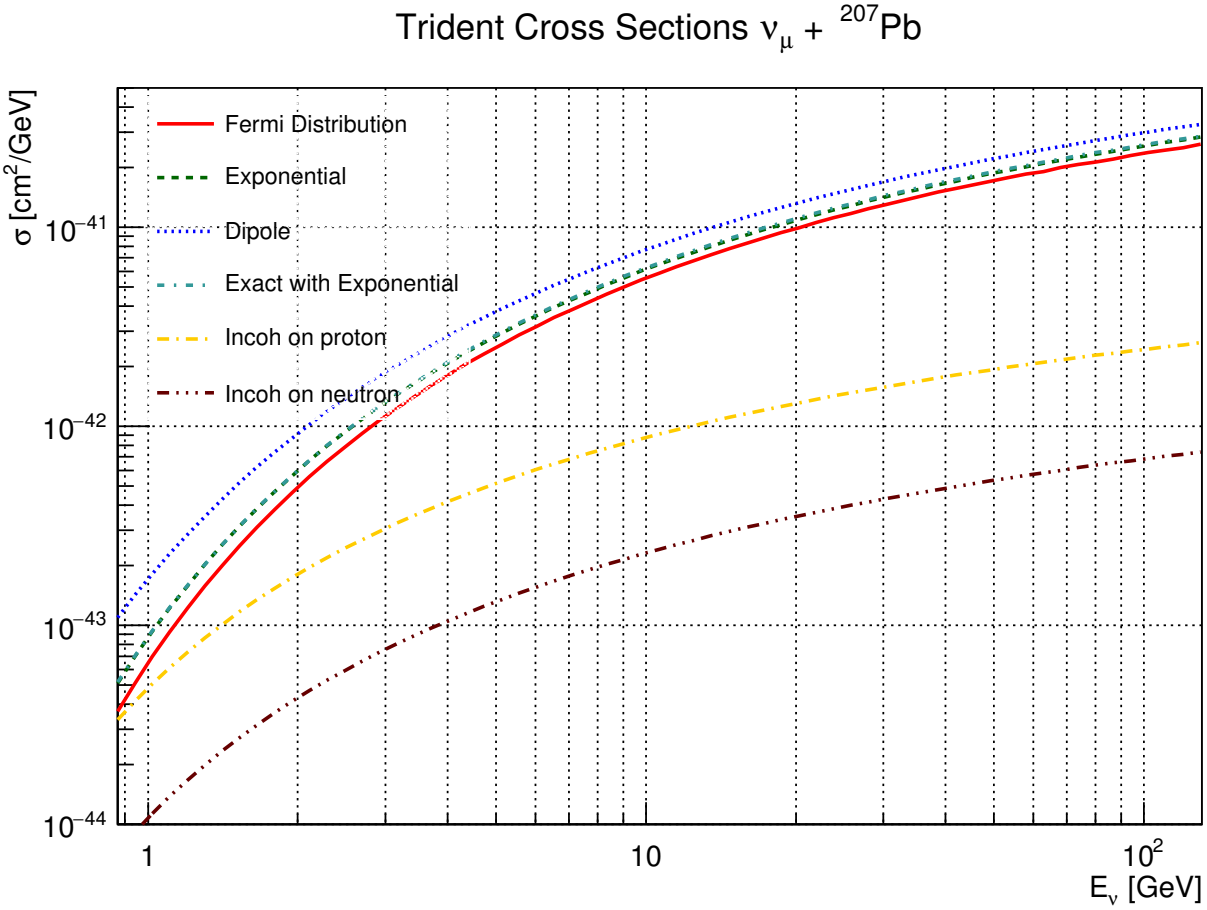

FIG. 4: Total cross section for process $\nu_\mu + {}^{207}Pb \to {}^{207}Pb + \mu^+ + \mu^- + \nu_\mu$ under several nuclear form factor parameterizations. Also shown are the incoherent process contributions from all protons and all neutrons and the exact cross section with exponential form factor. Plots for more elements can be found in appendix A

.

neutrino energy increases, inelastic and Deep Inelastic channels come into play [12]. However, for current accelerator-based neutrino beams, the second most relevant regime after the Coherent regime is the Incoherent regime, where the incoming neutrino is scattered off individual nucleons. Indeed, given the multi-particle final state of the trident process, it is unlikely to have enough momentum transfer to the target to reach the more extreme inelastic regimes. Incoherent processes are nevertheless tied to nuclear model assumptions. As pointed out in [29], these constitute the largest source of error in the trident calculation.

Two mayor nuclear effects can sensibly impact the Incoherent cross section calculation. First, due to the Pauli Exclusion principle, some final states may not be allowed. Second, the nucleon's initial Fermi motion has to be accounted for in the calculation. Pauli blocking can be roughly approximated by parameterizing the total trident cross section

$$d\sigma_{\text{tot}} = d\sigma_{\text{coh}} + X^{\text{excl}}(|\vec{q}|)\,[N d\sigma_{\text{n}} + Z, d\sigma_{\text{p}}] \tag{17}$$

where X^{excl} is an exclusion principle factor, as e.g. the one given by [4],

$$\begin{aligned} X^{\text{excl}}(|\vec{q}|) &= \begin{cases} 1.5\left(\frac{|\vec{q}|}{2p_f}\right) - 0.5\left(\frac{|\vec{q}|}{2p_f}\right)^3, & |\vec{q}| < 2p_f \\ 1, & \text{otherwise} \end{cases} \\ , p_f &= 235\text{MeV/c} \end{aligned} \tag{18}$$

which assumes an ideal Fermi Gas (FG) with the same density as that of protons in the nucleus [42]. Under the Fermi gas assumption, [28] finds that both effects are not interfering and concludes that Pauli Blocking alone accounts for

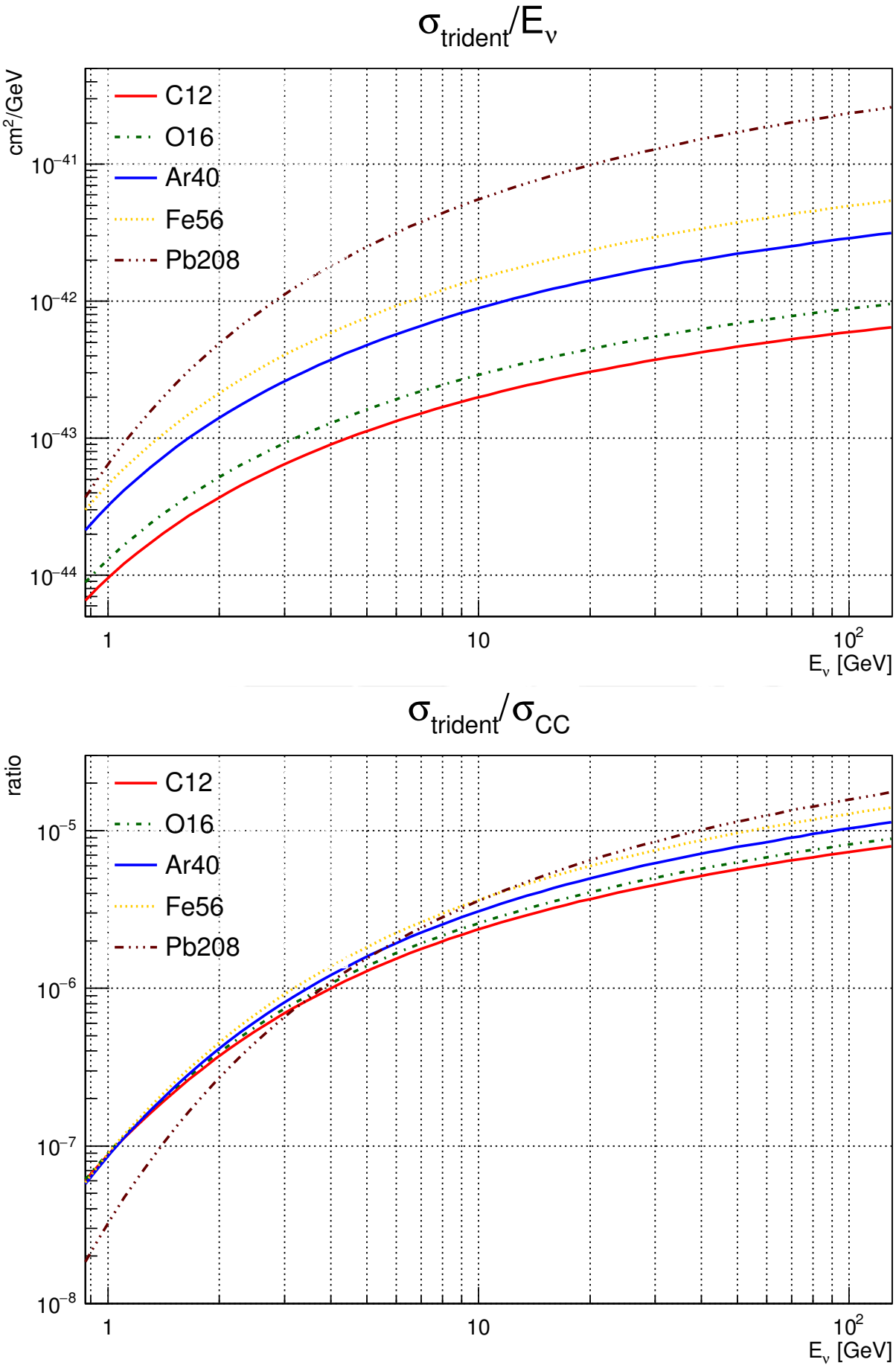

FIG. 5: Comparison of the total trident for different Z to inclusive CC cross sections for different nuclei.

a reduction of roughly 50% at high energies for protons and 20% for neutrons in the incoherent cross section. In our calculations, we have included Pauli blocking as stated in eq. 18. We show the total incoherent cross sections as defined in eq. 17 in figure 4 for ^{12}C and for other nuclei in appendix A. Incoherent contribution is small for protons and negligible for neutrons, due to the fact that these only couple through their magnetic moment.

C. Full calculation

According to eq. 2 the cross section in the SM has the form

$$\sigma^{SM} = C_V^2 \sigma_{C_V^2} + C_A^2 \sigma_{C_A^2} + C_V C_A \sigma_{C_V C_A}$$

Since the mixed term $\sigma_{C_V C_A}$ is about 2 orders of magnitudes smaller than the two others [5], it can be safely ignored. In many theoretical works also

$$\sigma_{C_A^2} \approx \sigma_{C_V^2} \tag{19}$$

is applied as motivated by the findings of Refs. [30]. Therefore, the full SM cross section can be retrieved from the pure V-A one via

$$\sigma^{SM} = \frac{1}{2}\left(C_V^2 + C_A^2\right)\sigma^{V-A}, \tag{20}$$

This fact is exploited by most theoretical works on trident production. However, Ref. [5] indicates that the approximation of eq. (19) is rather crude at small incident neutrino energies. We verified that this is not the case by calculating the exact matrix elements (eq. 5), using Feyncalc 9.0 [31, 32] for the trace reduction, and integrating the total cross section with the simple exponential form factor (see fig. 3). We found that both ways yield identical results; therefore in all previous and future calculations, we use equation 20 to compute the total SM cross section.

IV. SIMULATION FRAMEWORK

Our concern now turns to systematically studying the backgrounds of process 7 and exploring techniques allowing to improve the signal separation to the level required for NP searches in the context of non-oversimplified experiment simulations.

Due to the high statistics they can provide and their relatively well constrained neutrino flux, we focus on accelerator-based neutrino experiments. As current representative of these, we consider the on-axis spectral flux for the NuMI beamline in Medium Energy mode (fig. 6). We restrict to the most abundant neutrino species ($\nu\mu$).

We explore two widely used detector types: a Fine Grained organic scintillator Tracker (FGT) and a Liquid Argon Time Projection Chamber (LArTPC). In both types, the detector material serves both as primary scattering target and sensible element.

Our neutrino interaction simulation environment was GENIE v.2.12.4. For the signal process, we implemented a new event generation thread based on our trident cross section studies within this MC; while for the background generation, we rely on its default cross section models. Relevant background events were also propagated in our detector simulation using GEANT4[21] v.10.3.1.

We finally explore Multivariate Analysis (MVA) techniques by feeding experimental observables from signal and background processes into the TMVA[34] package v4.2.0 and examine both linear and non-linear classification algorithms. Conscious of real detectors limitations, we impose simple reconstruction efficiency cuts and analyze cases in which not all the observables are available.

A. Signal Events

The experimental signature of the trident process 7 comprises two oppositely charged muon-like particles originating from the same vertex. Also, the rapid fall of the nuclear form factor greatly limits the momentum transfer q, so a hadronic visible energy consistent with zero is also required. Regarding the kinematics, a very small invariant mass of the final-state lepton system is strongly enhanced in the process [3] and good reconstruction of very low muon momenta

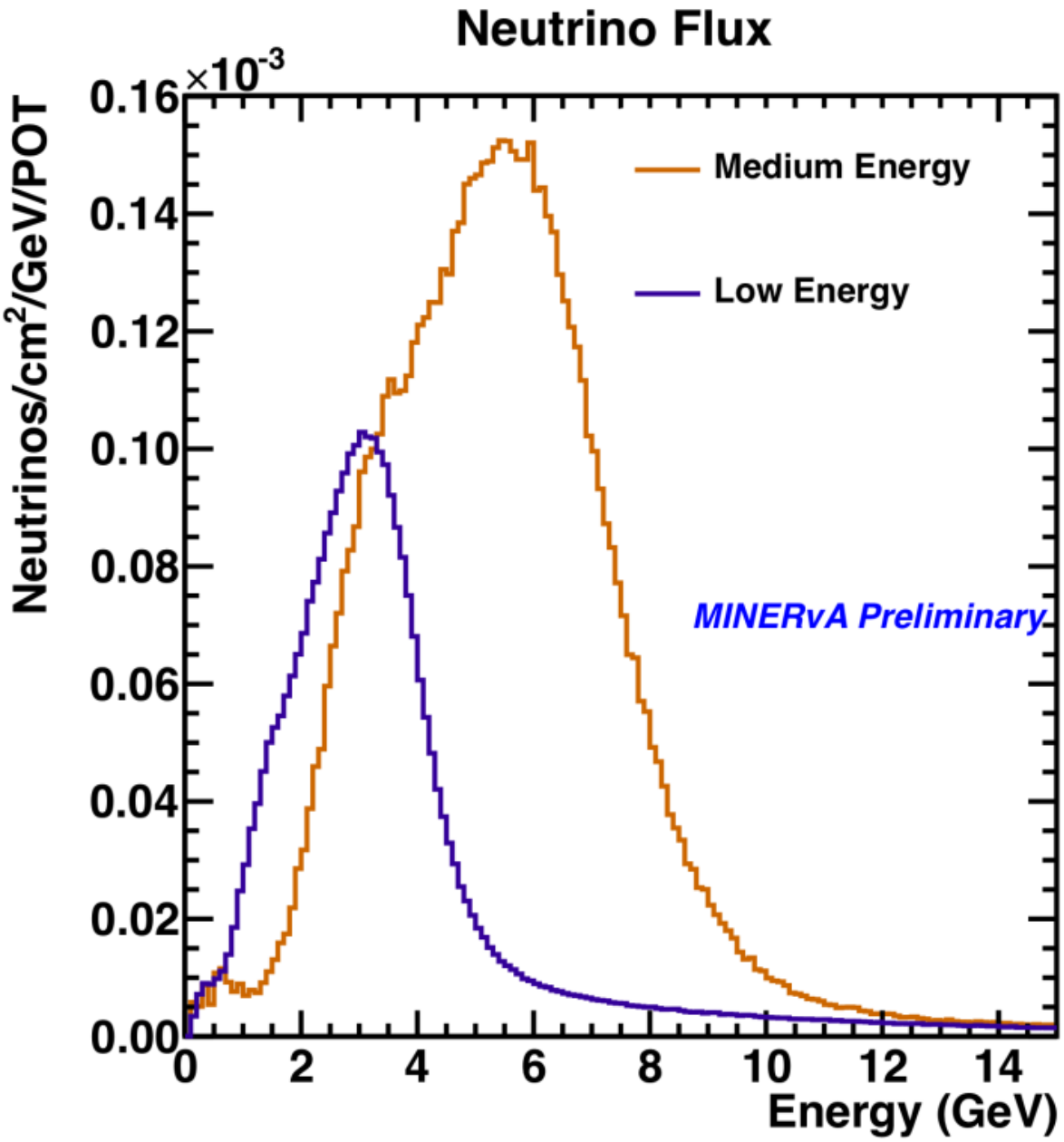

(a)

FIG. 6: NuMI muon neutrino fluxes 6a) Low and Medium Energy tunes (from ref. [33]).

(down to $\mathcal{O}$(MeV)) is anticipated to be necessary [4]. In spite of these requirements being restrictive, experimental measurements of trident must overcome the extremely small cross section, roughly 10^{-5} times the inclusive $\nu_\mu-$nucleon CC process, so the signal selection algorithm must be very efficient

In order to efficiently manage any trident related variable, we developed a new event generation thread for this process within GENIE which implements the SM contribution based on the $V-A$ cross section (eq. 20). The full code comprises the standard cross section, integrator, kinematics generator and final state particle generator modules. A detailed description of the code is to be found elsewhere [19].

As validation, we first used a Mathematica scripts to reproduce the total cross section full calculations from [1, 4] in the $V-A$ theory and from [5] in the SM. Our results also showed reasonable agreement with those of [6, 11] under the Equivalent Photon Approximation (EPA)[35, 36]. Then we calibrated our GENIE implementation to the Mathematica scripts.

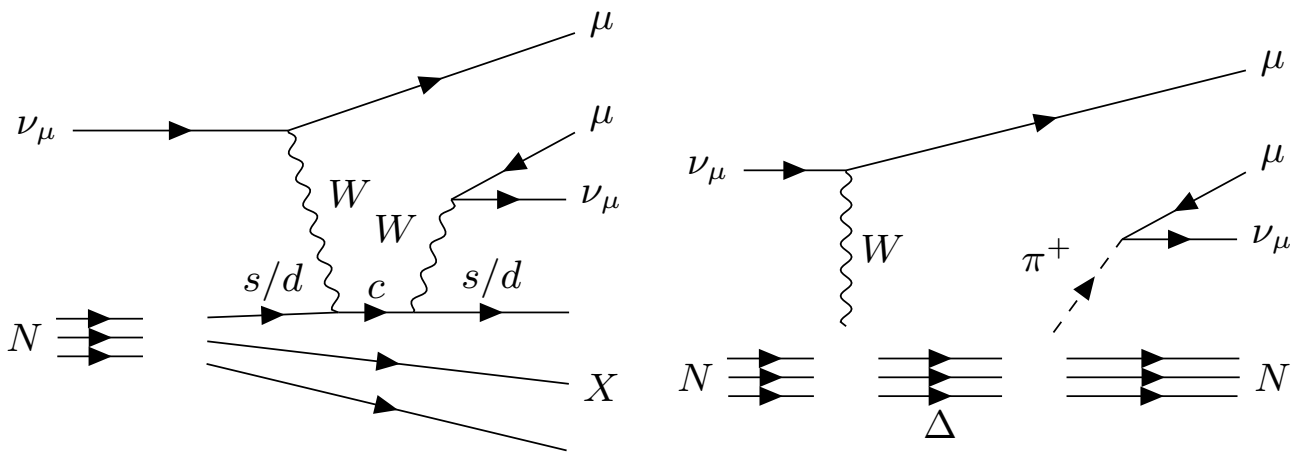

FIG. 7: Examples of possible di-muon diagrams by charm production and single pion production.

B. Backgrounds

Besides trident, in the SM there is a number of processes ressembling di-muon event. Most of these originate from the production and subsequent decay of some particle, like charm quarks or mesons. We make the general assumption that any of such processes exhibiting a hadronic shower can automatically be excluded.

1. *Charm Production*

Single charm production in CC neutrino nucleon interactions (fig. 7) with subsequent semileptonic decay of the charm quark

$$\begin{aligned} \nu_\mu + s/d \rightarrow \mu^\mp + c \\ c \rightarrow s/d + \mu^\pm + \nu_\mu \end{aligned} \tag{21}$$

yields opposite sign di-muons. In contrast to trident production, however, charm production is generally associated with a hadronic shower at the vertex [37], making both processes usually distinguishable.

There remains, nevertheless, the possibility of the excitation of a charmed resonance, e.g. a Λ_c^+. This process displays a more quasielastic-type behavior. Due to its short lifetime (around 2×10^{-13} s [38]), a Λ_c^+ decays quite quickly in a detector. One possible decay channel is into a neutrino, a neutron and a muon. However, depending on the detector, the visibility of neutrons is still a topic under study.

Under the hadronic shower distinguishability criteria, we simulated charged current charm production events, excepting DIS channels. Specifically, this was realized by using the *Quasielastic-Charm* event generation thread in GENIE. All of these events were considered as background for subsequent analysis.

2. *Pion Production*

Inclusive charged pion production, with subsequent decay of the pion into a muon and a neutrino

$$\begin{aligned} \nu_\mu + N \rightarrow \mu^\mp + X + \pi^\pm \\ \pi^\pm \rightarrow \mu^\pm + \nu_\mu \end{aligned} \tag{22}$$

may give the same final state as Coherent trident, depending on a complex combination of the specific interaction channel by which a pion was produced and Final State Interactions (FSI).

This background may be excluded by topology alone whenever the pion lives long enough to leave a track and this track is not misreconstructed as a single one with that of the muon coming from its decay. In addition, a charged pion escaping the detector before decaying or interacting can easily fake a muon; due to its similar mass, energy deposition is not reliable in this case.

TABLE I: Observables considered for the analysis

Observable	Description	Reconstruction Requirements
Z_{int}	Longitudinal position of interaction vertex	Vertexing
θ_+	Track polar angle of positive particle (w.r.t. beam axis)	Tracking, charge ID
θ_-	Track polar angle of negative particle (w.r.t. beam axis)	Tracking, charge ID
θ_{+-}	Angular separation between positive and negative particle tracks	Tracking
E_{+-}	Energy difference between positive and negative particles	Muon calorimetry (charge ID for sign)
W_{+-}	Invariant mass of positive and negative particles	Full muon momentum

The pion production background was accounted for by generating an inclusive sample of charged current events and selecting the ones having a single charged pion in the final state. Specifically, the event generation was set up for all charged current non-DIS channels, which include channels capabel of producing sinlge pions indiretcly like quasielastics and resonance excitations, as well as channels directly producing pions, like the Coherent production (Berger-Sehgal model [39]) and Diffractive production (Rein model [40]).

Then, the pions from single pion events were propagated in detector simulations described below and events being either

- passing-through pion events: when pion escapes the detector
- small-angle pion decay events: when pion decays making an angle less than 0.5 degrees with its daughter muon

were considered as background events for subsequent analysis.

3. Other sources

Neutral current diffractive J/ψ production and decay to $\mu^+\mu^-$ was e.g. considered by CCFR [41] and excluded by removing candidates with di-muon invariant mass around the peak for J/ψ production (3.1 ± 0.4 GeV). As the trident invariant mass distribution was found to be strongly suppressed above just one GeV, this channel was not included in our treatment of backgrounds.

4. Propagation simulation

Since particularly the pion production background originates from the propagation of pions within a detector, it was deemed appropriate to simulate this propagation through a medium similar to the one that would be present in a real-life detector. This was carried out in Geant4 and received the input of events produced using GENIE. Each pion, with its respective GENIE-generated momentum was placed at a random longitudinal position inside the detector's fiducial volume and propagated along the whole detector volume.

We considered a MINERνA-like geometry simulation, consisting of a cylinder shaped volume of plastic (CH) material. This volume was divided in 111 discoidal modules, each of 2m radius, 18mm height and leaving a 7mm separation between modules. Each of this modules further comprised two scintillator planes, with 2mm separation between them. As fiducial volume, we established a cylinder-shaped volume centered in the main volume and having 1m radius and 2.5m length.

V. ANALYSIS METHODS

Once both signal and background events were generated and preselected as described above, we implemented the following analysis to attempt to separate them, our aim being to extract as much of the remaining information as possible from the event kinematics.

We define six experimental observables, as listed in table I. Recall that all of the trident candidates have the minimum topology requirement of two muon-like tracks originating at the same point, i.e., vertex reconstruction is already guaranteed in the considered types of detectors.

With this observables in mind, we explored a number of MVA classification techniques available through the TMVA package. We expected non-linear methods to perform better, given the complex correlations among our input variables, shaped by both kinematical and highly non-trivial dynamical relationships. Thus for comparison, in exploratory assays

TABLE II: Studied scenarios of availability of observables

Scenario	Available observables						# of vars
1		θ_+	θ_-	θ_{+-}	E_{+-}	W_{+-}	5
2		θ_+	θ_-	θ_{+-}	E_{+-}		4
3	Z_{int}	θ_+	θ_-	θ_{+-}			4
4	Z_{int}	θ_+	θ_-				3
5	Z_{int}	θ_+					2
6				θ_{+-}	$\lvert E_{+-}\rvert$	W_{+-}	3
7				θ_{+-}	$\lvert E_{+-}\rvert$		2
8	Z_{int}			θ_{+-}			2
9		θ_+	θ_-	θ_{+-}			3
10		θ_+	θ_-				2

we applied an intrinsically linear classifier (Linear Discriminant with prior decorrelation via Principal Components), a non-linearized linear classifier (Boosted Fisher) and intrinsically non-linear classifiers (k-Nearest Neighbors, Boosted Neural Networks and Boosted Decision Trees). We briefly describe here the two methods whose results we report in section VI:

- Boosted Fisher (BF): The base linear method optimizes class separation with a hyperplane in the phase space. It is non-linearized through the application of a general purpose MVA Boosting scheme (Adaptive Boost [34]).
- Boosted Decision Trees (BDT): A generalization of the concept of rectangular cuts to subregions of the phase space through the same general purpose MVA Boosting scheme.

Acknowledging the possible variations within the two general detector types we study, we have further examined a series of scenarios, listed in table II, in which different combinations of observables are available. The ordering for observable removal was first driven by experimental reconstruction requirements and then by classification power of observables and correlations as obtained in exploratory assays.

For each scenario, the complete TMVA cycle of training, testing and evaluation was run. In scenarios where muon calorimetry is implied (i.e., when E_{+-} or W_{+-} are present), it is assumed that pions are tagged in calorimeters as they interact leaving a shower. Therefore, the passing-through pions background is excluded from this scenarios and Z_{int} is accordingly not considered as it is uniform for the rest of the processes.

Scenarios 1 through 5 assume charge ID is available, which is typically realized with a strong enough magnetic field. In contrast, scenarios 6 through 8 assume no charge ID. Finally, scenarios 9 and 10 correspond to the purely angular case with charge ID. Recall that in a real-life detector, different individual scenarios may be recreated in determinate subregions or situations.

Before proceeding any further, it is noteworthy that we generated enough events of each kind of process for the distributions of the observables to be smooth, i.e., until the space of observables becomes sufficiently populated. During the analysis, naturally, event channels were reweighted to their physical ratios.

VI. RESULTS

In the following we summarize the results of our analysis. First, we examine the distributions of all the observables used in the MVA (figure 8). Background in this graphics includes Quasielastic-charm and Small-angle pion backgrounds and is largely shaped by the latter owing to their much higher physical probability of occurrence. The Passing-pions background is only included in the distributions of Z_{int}, as this variable is only relevant for this type of background.

As expected, the invariant mass is seemingly the variable exhibiting the best separation power, followed by the θ_+ and, notoriously later, θ_-. This asymmetry can be explained thanks to the fact that in trident events the momentum transfer is small, so the outgoing μ^- carries almost entirely the incoming ν momentum, while for background processes, the μ^+ comes from the decay of another particle, so again, most of the incoming ν momentum is carried by the μ^-. Separation power seems to be low for E_{+-} (or $|E_{+-}|$). Z_{int} might be useful in the absence of other variables, particularly because it is always available.

Exploratory assays to determine potentially superfluous variables showed some correlation between E_{+-} and θ_{+-} with the other angular variables. In the analyzed scenarios, θ_{+-} is removed first as more information is expected to be contained in θ_+ and θ_- together.

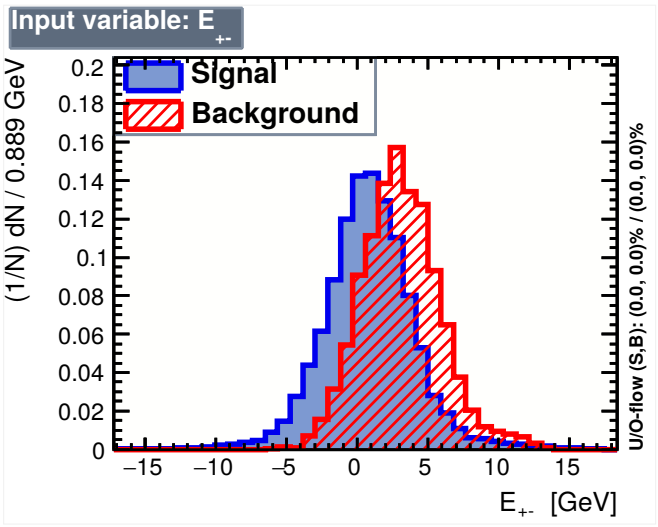

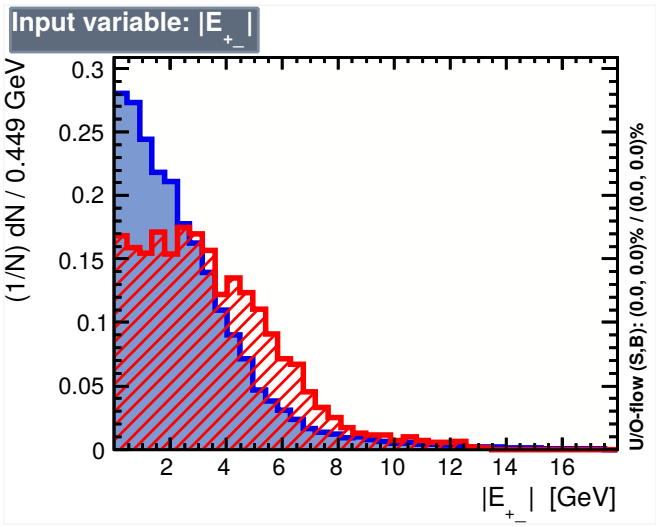

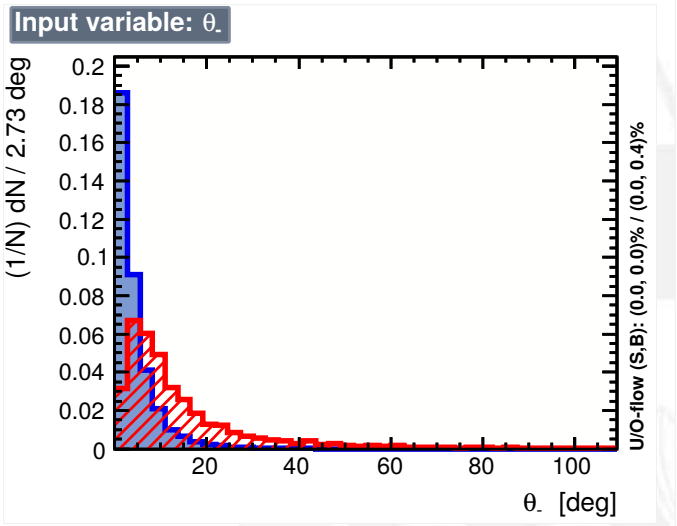

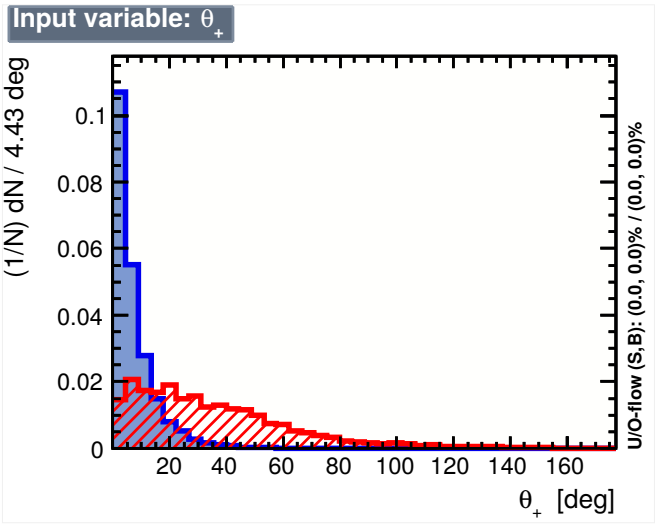

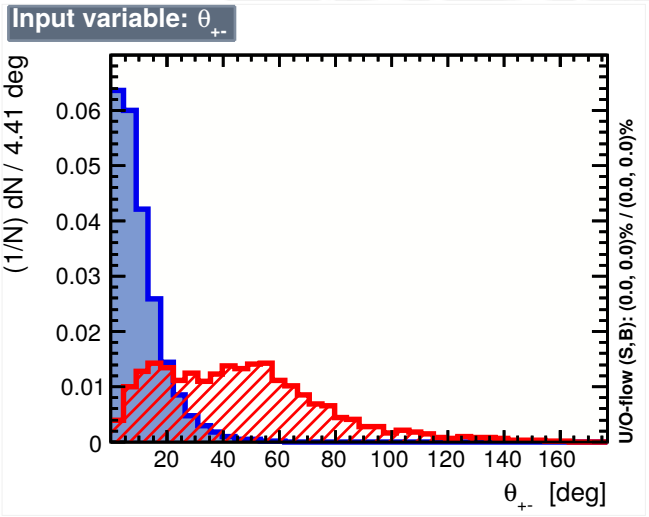

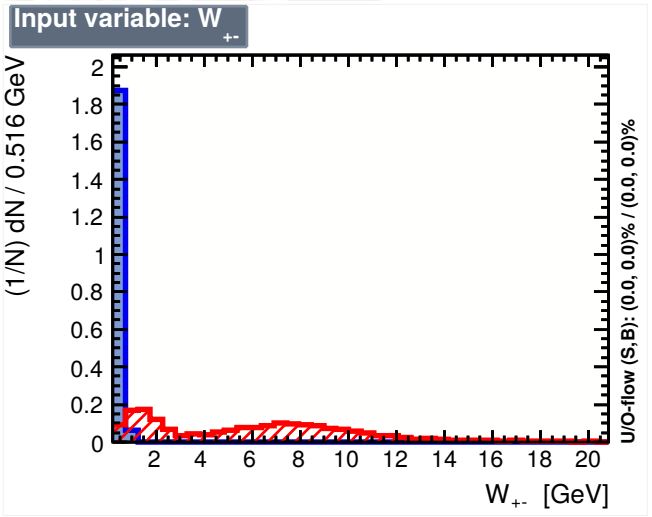

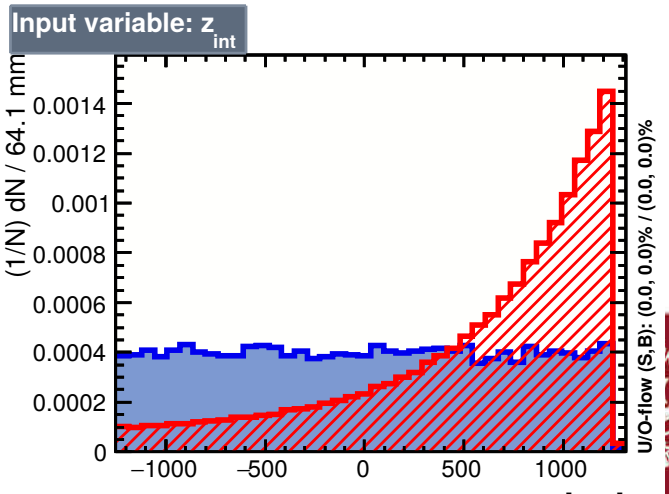

For comparing the performance of classifiers, we include the separation and significance, as defined in [34], of the methods for each scenario (fig. 9). A notorious decrease in method performance is observed whenever the invariant mass is retired from the analysis (compare scenarios 1 and 6 vs. the rest). Also, we note that including the energy difference (scenarios 1,2,6 and 7) does not seem to make a great improvement over the more restricted scenarios. Furthermore, as assuming the energy difference can be computed implies that the invariant mass can also be, this only adds to the importance of this latter observable.

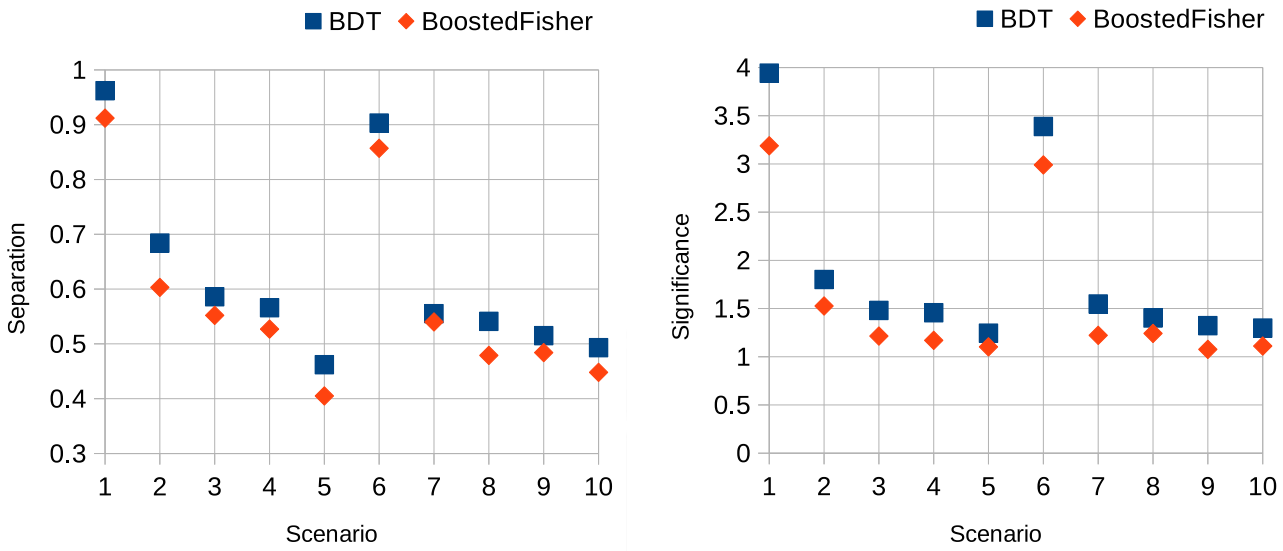

(a) Separation (b) Significance

FIG. 9: Comparison of MVA classifiers overall performance in each scenario.

We also signal another important decrease in separation power when θ_- is removed from analysis (compare scenarios 5 vs. 4). The purely angular scenarios (9 and 10) show worse performance in general.

Regarding the methods themselves, it is noteworthy how the boosting scheme improved the Fisher classifier to the point of being competitive to BDT. In appendix B, we show the classifier output distributions for both training and testing samples to check that methods were not overtrained, which is particularly a concern for BDT. We also include the signal and background efficiencies vs. cut values for both methods. The boosting of the Decision Trees method was also monitored to ensure proper development of the forest.

VII. CONCLUSIONS

We have implemented a detailed simulation of the trident process and reanalyzed the background processes within the GENIE and GEANT4 current framework. We have chosen for the neutrino flux the Medium Energy tune of the NuMI beam. This one illuminates a detector simulation that assumes a carbon detector material, mimicking at some level a MINERνA-like scenario and one of the options for the DUNE Near Detector-like scenario. We have performed the signature optimization with the BDT multivariate analysis method. Our results indicate that, for the NuMI ME flux and a carbon detector, the invariant mass is the best observable for signal and background discrimination, reaching up to 4σ when all the observables are available.

Acknowledgments

This work has been supported by Cienciactiva-CONCYTEC, DGI-PUCP and Fermilab NPC. Authors would like to thank W. Altmannshofer for many illustrating suggestions on trident production and the MINERνA collaboration for the hospitality extended to J.B. and S.S. during their stay therein. One of the authors (S.S.) would like to thank E. Sánchez for his advice on the statistical treatment.

Appendix A: Form Factor Effects in the Total Cross Section of Coherent Process, different Nuclei

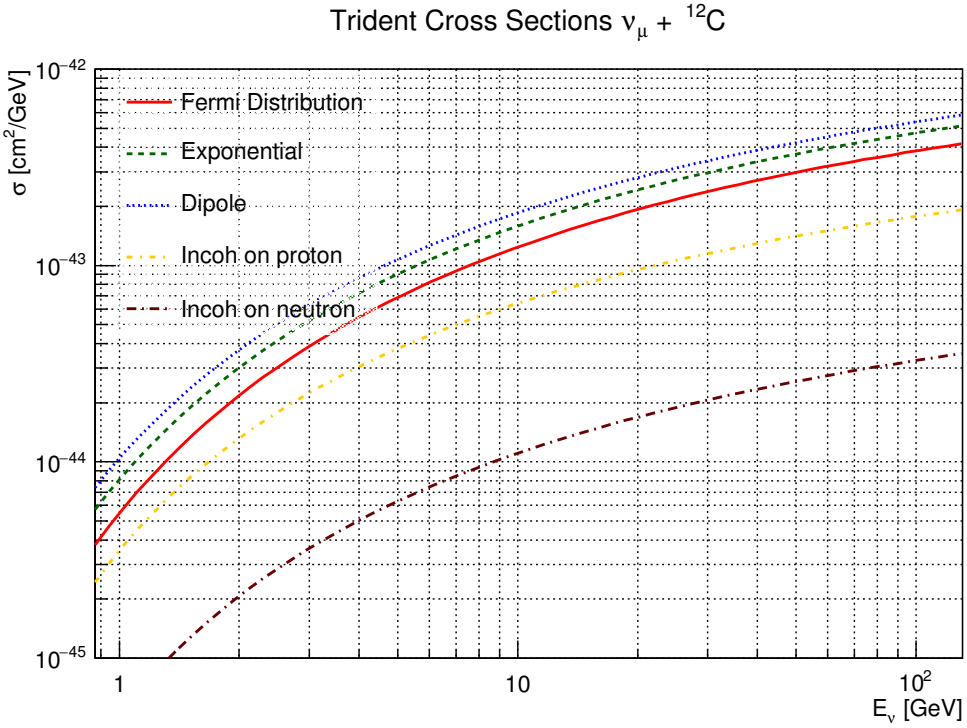

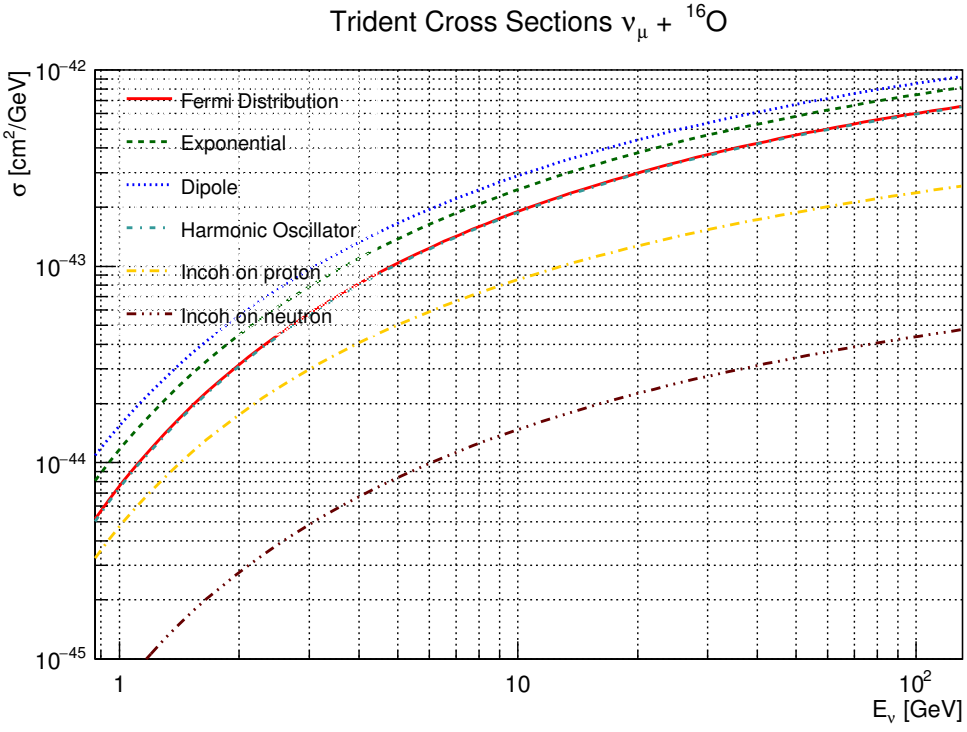

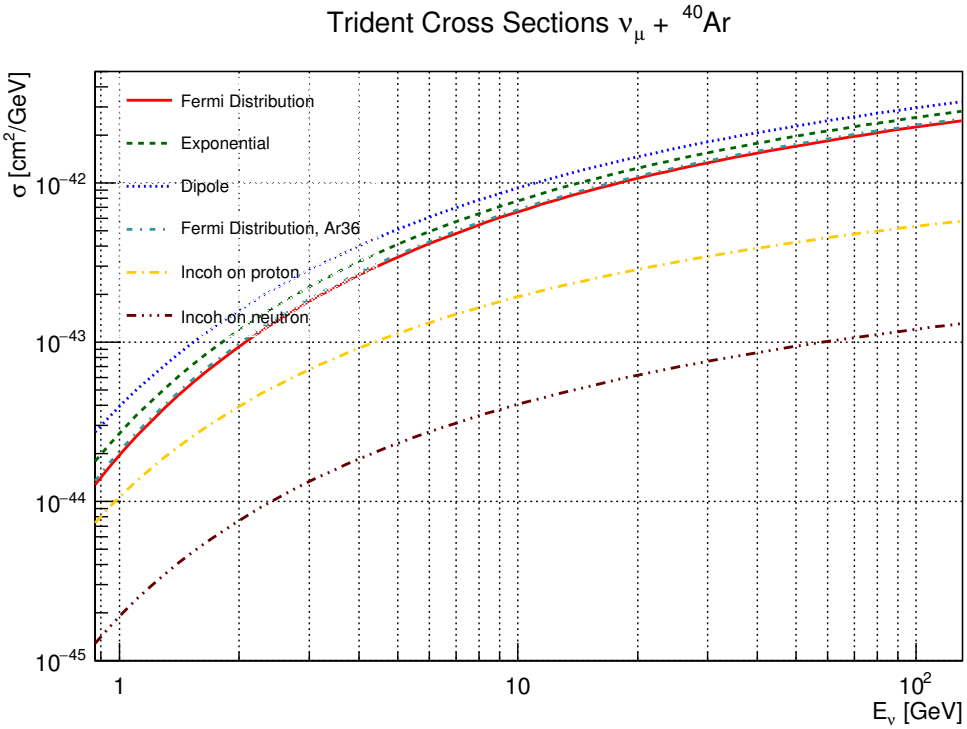

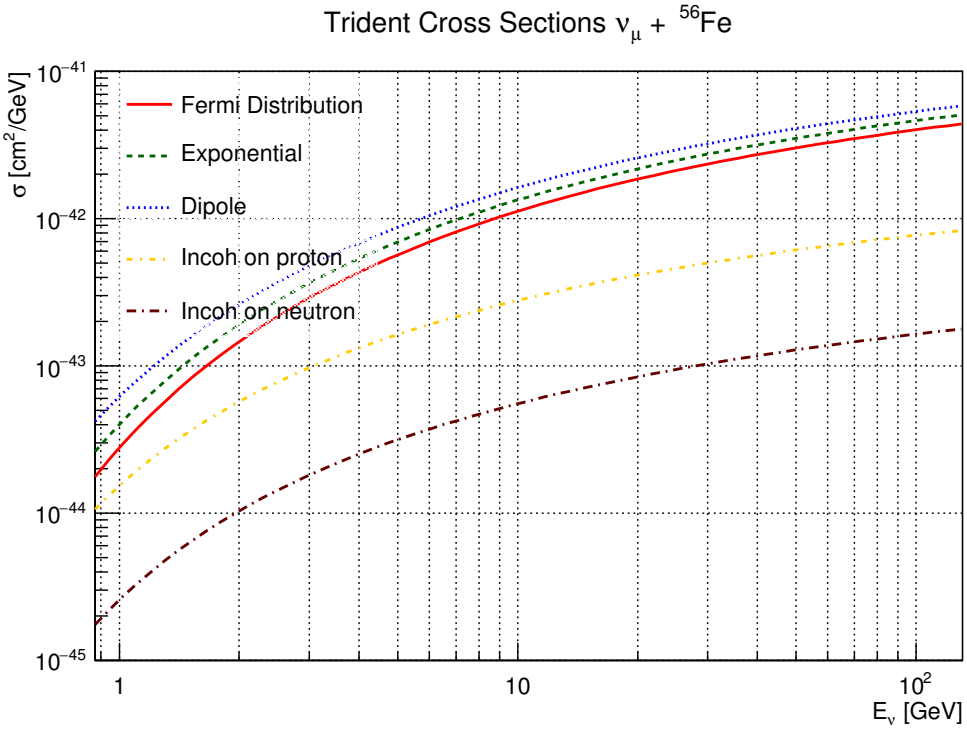

Appendix B: MVA Overtraining and Cut Values Plots

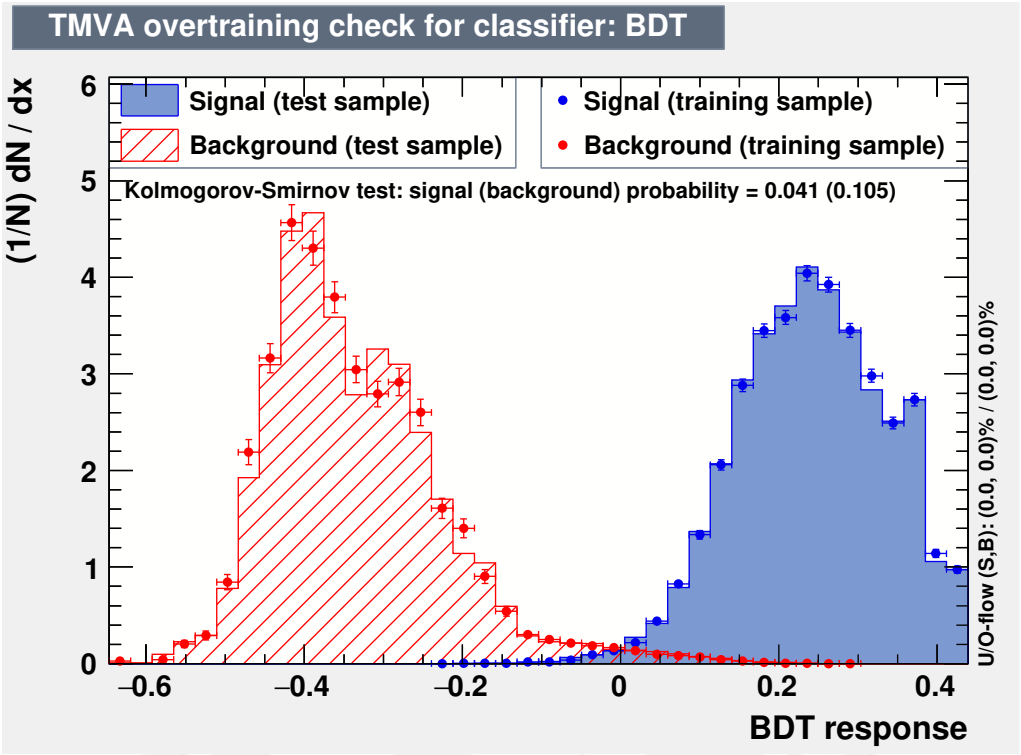

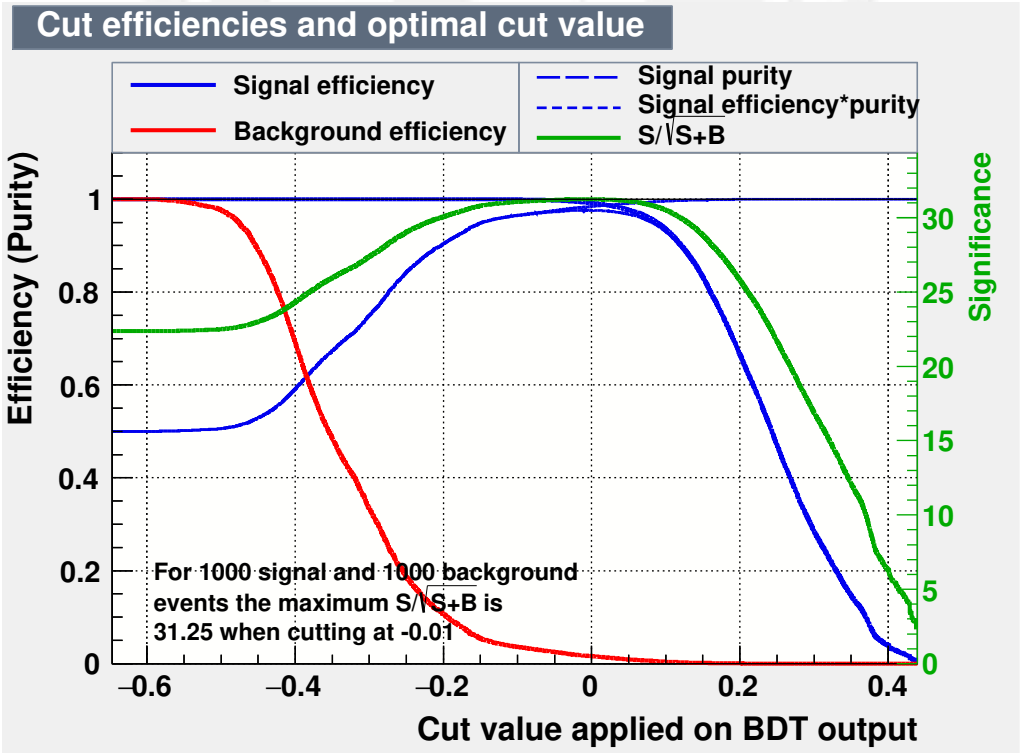

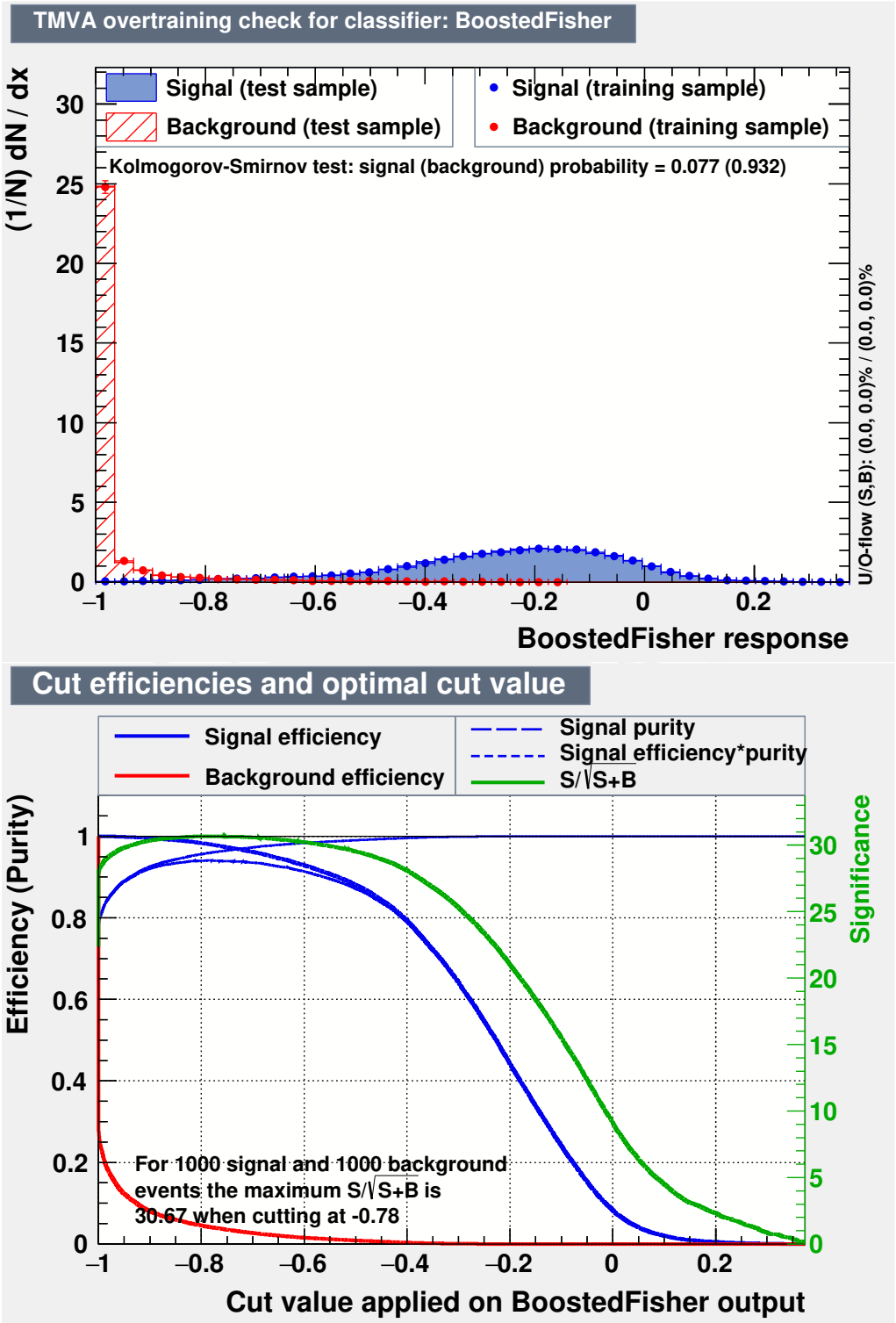

[1] W. Czyz, G. C. Sheppey, and J. D. Walecka. Neutrino production of lepton pairs through the point four-fermion interaction. *Nuovo Cim.*, 34:404–435, 1964.

[2] M.S. Marinov, P. Nikitin, Y. P. Orevkov, and E. P. Shabalin. Direct production of lepton pairs by a neutrino beam in the electromagnetic field of a nucleus. *Sov. J. Nucl. Phys*, 3:497–503, 1966.

[3] K. Fujikawa. The self-coupling of weak lepton currents in high-energy neutrino and muon reactions. *Annals Phys.*, 68:102–162, 1971.

[4] J. Lovseth and M. Radomiski. Kinematical distributions of neutrino-produced lepton triplets. *Phys. Rev.*, D3:2686–2706, 1971.

[5] R. W. Brown, R. H. Hobbs, J. Smith, and N. Stanko. Intermediate boson. iii. virtual-boson effects in neutrino trident production. *Phys. Rev.*, D6:3273–3292, 1972.

[6] R. Belusevic and J. Smith. W - Z Interference in Neutrino - Nucleus Scattering. *Phys. Rev.*, D37:2419, 1988.

[7] F. Bergsma et al. Search for Coherent Muon Pair Production by Neutrinos and Anti-neutrinos. *Phys. Lett.*, B122:185, 1983.

[8] D. Geiregat et al. First observation of neutrino trident production. *Phys. Lett.*, B245:271–275, 1990.

[9] B. A. Schumm et al. Search for neutrino trilepton production in the Fermilab Tevatron neutrino beam by the CCFR Collaboration. In *'88 electroweak interactions and unified theories. Proceedings, 23rd Rencontres de Moriond, Leptonic Session, Les Arcs, France, March 6-13, 1988*, pages 413–420, 1988.

[10] T. Adams et al. Neutrino trident production from NuTeV. In *High-energy physics. Proceedings, 29th International Conference, ICHEP'98, Vancouver, Canada, July 23-29, 1998. Vol. 1, 2*, pages 631–634, 1998.

[11] Wolfgang Altmannshofer, Stefania Gori, Maxim Pospelov, and Itay Yavin. Neutrino Trident Production: A Powerful Probe of New Physics with Neutrino Beams. *Phys. Rev. Lett.*, 113:091801, 2014.

[12] Gabriel Magill and Ryan Plestid. Neutrino Trident Production at the Intensity Frontier. *Phys. Rev.*, D95(7):073004, 2017.

[13] P. Adamson et al. The NuMI Neutrino Beam. *Nucl. Instrum. Meth.*, A806:279–306, 2016.

[14] James Strait et al. Long-Baseline Neutrino Facility (LBNF) and Deep Underground Neutrino Experiment (DUNE). 2016.

[15] J. Nelson. Neutrino-nucleus scattering results from MINERvA, part 1. In *18th International Workshop on Neutrino Factories and Future Neutrino Facilities Search (NuFact16) Quy Nhon, Vietnam, August 21-27, 2016*, 2016.

[16] R. Acciarri et al. Long-Baseline Neutrino Facility (LBNF) and Deep Underground Neutrino Experiment (DUNE). 2015.

[17] L. Aliaga et al. Design, Calibration, and Performance of the MINERvA Detector. *Nucl. Instrum. Meth.*, A743:130–159, 2014.

[18] R. Acciarri et al. Long-Baseline Neutrino Facility (LBNF) and Deep Underground Neutrino Experiment (DUNE). 2016.

[19] S.Sánchez Falero, E. Endress, J.Becerra, and A.M.Gago. Implementation and validation of Neutrino Trident Production Processes in the GENIE Neutrino MC Generator. In preparation.

[20] Costas Andreopoulos, Christopher Barry, Steve Dytman, Hugh Gallagher, Tomasz Golan, Robert Hatcher, Gabriel Perdue, and Julia Yarba. The GENIE Neutrino Monte Carlo Generator: Physics and User Manual. 2015.

[21] S. Agostinelli et al. GEANT4: A Simulation toolkit. *Nucl. Instrum. Meth.*, A506:250–303, 2003.

[22] H. H. Chen and B. W. Lee. Experimental tests of weinberg's theory of leptons. *Phys. Rev.*, D5:1874–1877, 1972.

[23] G. Peter Lepage. A New Algorithm for Adaptive Multidimensional Integration. *J. Comput. Phys.*, 27:192, 1978.

[24] T. Hahn. CUBA: A Library for multidimensional numerical integration. *Comput. Phys. Commun.*, 168:78–95, 2005.

[25] GSL Project Contributors. GSL - GNU scientific library - GNU project - free software foundation (FSF). http://www.gnu.org/software/gsl/, 2010.

[26] H. De Vries, C. W. De Jager, and C. De Vries. Nuclear charge and magnetization density distribution parameters from elastic electron scattering. *Atom. Data Nucl. Data Tabl.*, 36:495–536, 1987.

[27] M. E. Grypeos, G. A. Lalazissis, S. E. Massen, and C. P. Panos. The 'COSH' or symmetrized Woods-Saxon nuclear potential. *Submitted to: J. Phys. G*, 1991.

[28] R. W. Brown and J. Smith. Intermediate boson. i. theoretical production cross-sections in high-energy neutrino and muon experiments. *Phys. Rev.*, D3:207–223, 1971.

[29] S. R. Mishra et al. Recent electroweak results from the CCFR Collaboration: Neutrino tridents and W - Z interference and the Lorentz structure of the weak current. In *Electroweak interactions and unified theories. Proceedings, Leptonic Session of the 26th Rencontres de Moriond, Les Arcs, France, March 11-17, 1991*, pages 87–96, 1991.

[30] K. Fujikawa. Effects of the neutral weak current on the process $\nu + (Z) \to \nu + \mu + \bar{\mu} + (Z)$. *Phys. Rev.*, D8:1623–1626, 1973.

[31] R. Mertig, M. Bohm, and Ansgar Denner. FEYN CALC: Computer algebraic calculation of Feynman amplitudes. *Comput. Phys. Commun.*, 64:345–359, 1991.

[32] Vladyslav Shtabovenko, Rolf Mertig, and Frederik Orellana. New Developments in FeynCalc 9.0. *Comput. Phys. Commun.*, 207:432–444, 2016.

[33] Laura Fields. Recent Results from MINERvA. In *27th International Conference on Neutrino Physics and Astrophysics (Neutrino 2016) London, United Kingdom, July 4-9, 2016*, 2016.

[34] Andreas Hoecker, Peter Speckmayer, Joerg Stelzer, Jan Therhaag, Eckhard von Toerne, and Helge Voss. TMVA: Toolkit for Multivariate Data Analysis. *PoS*, ACAT:040, 2007.

[35] C. F. von Weizsacker. Radiation emitted in collisions of very fast electrons. *Z. Phys.*, 88:612–625, 1934.

[36] E. J. Williams. Nature of the high-energy particles of penetrating radiation and status of ionization and radiation formulae. *Phys. Rev.*, 45:729–730, 1934.

[37] H. Abramowicz et al. Experimental Study of Opposite Sign Dimuons Produced in Neutrino and anti-neutrinos Interactions. *Z. Phys.*, C15:19, 1982.

[38] C. Patrignani et al. Review of Particle Physics. *Chin. Phys.*, C40(10):100001, 2016.

[39] Ch. Berger and L. M. Sehgal. Partially conserved axial vector current and coherent pion production by low energy neutrinos. *Phys. Rev. D*, 79:053003, Mar 2009.

[40] D. Rein. Diffractive Pion Production in Neutrino Reactions. *Nucl. Phys.*, B278:61–77, 1986.

[41] S. R. Mishra et al. Neutrino tridents and W Z interference. *Phys. Rev. Lett.*, 66:3117–3120, 1991.
[42] The formula without this factor can be derived on the assumption that the nucleons in the nucleus can not move and have uncorrelated positions. Here, the Fermi motion of the nucleons is still ignored but we allow for the correlation implied by the exclusion principle

Neutrino Trident Production revisited for DUNE-like and MINERvA-like scenarios

Sebastián Sánchez

in collaboration with J. Becerra, E. Endreß, A. Gago

Sección Física, Departamento de Ciencias, Pontificia Universidad Católica del Perú, Apartado 1761, Lima, Perú

Friday, May 19th, 2017

Contents

Introduction

We revisit **neutrino trident production**:

- neutrino production of lepton triplets in the Couloumb field of nuclei
- has been extensively studied in the past [1, 2, 3, 4, 5, 6]
- can occur via Charged Current (CC) or Neutral Current (NC)
- one of the few SM processes allowing to directly test $W - Z$ interference

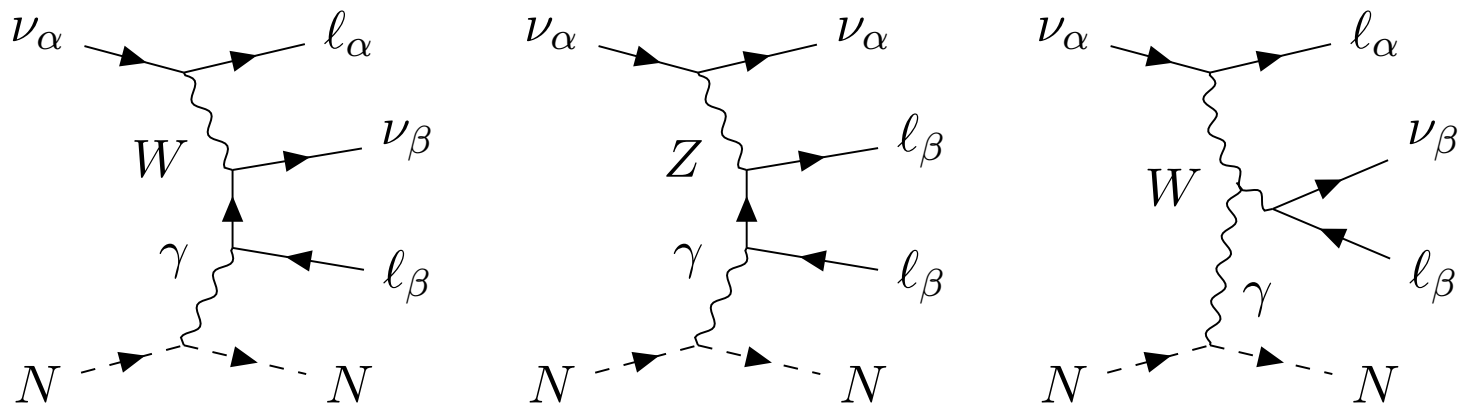

Figure: Tree-level trident Feynman diagrams, for $\alpha, \beta = e, \mu, \tau$.

Difficult, but not impossible to observe:

- small cross sections $\sim 10^{-5}$ times the inclusive ν_μ nucleon CC for incoming neutrino energies up to $O(100\ \text{GeV})$
- but clear experimental signature for $\alpha = \beta = \mu$: recoilless dimuon events
- first evidences by CHARM[7] then first cross section measurement by CHARM II [8], with $\langle E_\nu \rangle \sim 160$ GeV on Fe
- measurement by CCFR [9], with $\langle E_\nu \rangle \sim 20$ GeV on SiO_2, finally able to rule out pure $V - A$ at 95% C.L.

All measurements consistent with SM:

$$\begin{aligned} \sigma_{\text{CHARM-II}}/\sigma_{\text{SM}} &= 1.58 \pm 0.57, \\ \sigma_{\text{CCFR}}/\sigma_{\text{SM}} &= 0.82 \pm 0.28 \end{aligned}$$

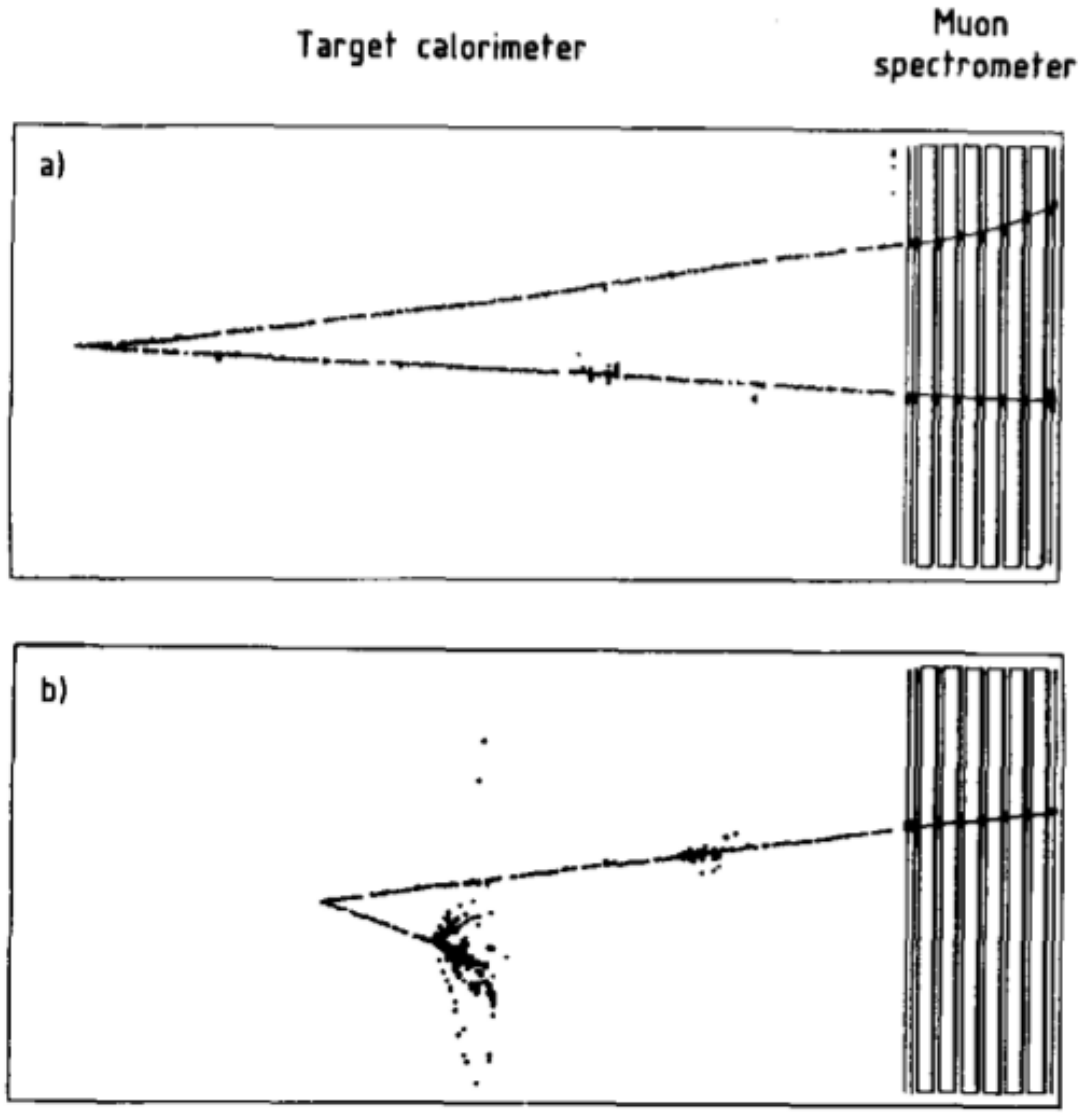

Figure: Trident candidate vs. Background from CHARMII [8] event display

Trident saw a revived interested recently as probe for New Physics (NP):

- a model studied by Altmannshofer et al.[10] comprises a new neutral current among lepons due to gauge symmetry in $L_\mu - L_\tau$
- the corresponding vector boson Z' would interfere with SM bosons W and Z and modify the trident event expectancy by a sizable amount

To conclusively observe this effects, we need to clearly separate the scarce trident events from SM backgrounds:

- Deep Inelastic Scattering (DIS)
- Charm production
- Resonance Excitations
- CC Inclusive Single Pion production

Most trident searches rely on event topology and invariant mass

We study the factibility of improving event discrimination with MultiVariate Analysis (MVA) methods and in non-oversimplified accelerator-based experimental frameworks

- neutrino flux: NuMI[11] in the Medium Energy tune has $\langle E_\nu \rangle \sim 6$ GeV) and is expected to deliver $\sim 4 \times 10^{21}$ POTs over course of 2 years [12]
- detector simulation: segmented carbon target, mimicking a fine grained scintillator like MINERνA[13] or one of the options for DUNE ND [14]

, with a detailed simulation of the trident process in GENIE [15] and a reanalysis of relevant backgrounds, using GENIE and GEANT4 [16].

Theoretical aspects

- Iteraction with target is purely EM, thus no hadronic physics obscuring the weak part [4]
- Low energy threshold, $E_\nu^{\text{thr}} = 3m + 2m^2/M_{Target}$
- Not kinematically limited upwards, as e.g. muon decay

At accelerator neutrino beams, we are sufficiently below Glashow resonance, so an effective lagrangian is used

$$\mathcal{L} = \frac{G_F^2}{\sqrt{2}} \bar{\mu}\gamma_\alpha \left(C_V - \gamma_5 C_A\right) \mu \bar{\nu}\gamma^\alpha \left(1 - \gamma_5\right) \nu \tag{1}$$

Recall this already is an admixture of CC and NC

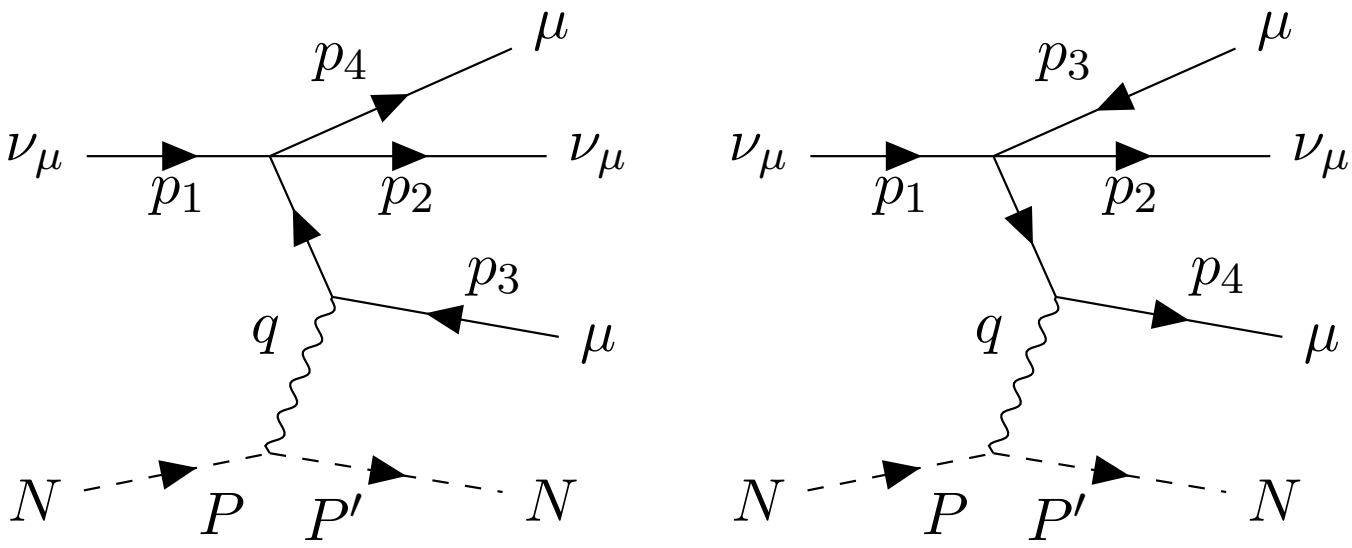

Figure: 4 point effective diagrams and momenta label convention

Under single photon exchange, $|\mathcal{M}^2|$ for trident factorizes in a leptonic and an hadronic part, thus [6]

$$\sigma^{SM} = C_V^2 \sigma_{C_V^2} + C_A^2 \sigma_{C_A^2} + C_V C_A \sigma_{C_V C_A} \tag{2}$$

Explicitly, the trident cross section [1] is

$$\sigma^{SM} = \frac{2Z^2\alpha^2 G_F^2}{(2\pi)^6}\frac{1}{4M_T E_1}\int \frac{d^3P'}{2E'}\,\mathcal{F}_{\mu\nu}(P,q)\,\mathcal{L}^{\mu\nu}(p_1,q)\,\frac{1}{q^4}, \qquad (3)$$

where M_T is target mass, E' the final target energy and $q = P - P'$ the momentum transfer to the nucleus.
The leptonic contribution

$$\mathcal{L}_{\mu\nu} = \int \frac{d^3p_2}{2E_2}\int \frac{d^3p_3}{2E_3}\int \frac{d^3p_4}{2E_4}\,\delta^4\left(q + p_1 - p_2 - p_3 - p_4\right)\mathcal{M}_{\mu\nu} \qquad (4)$$

Finally, the hadronic part [1] for a spin-0 nuclear target

$$\begin{aligned}\mathcal{F}_{\mu\nu}(P,q) &= \mathcal{F}_{\nu\mu}(P,q)\\ &= 4|F(q^2)|^2\left(P_\mu - \frac{1}{2}q_\mu\right)\left(P_\nu - \frac{1}{2}q_\nu\right)\end{aligned} \qquad (5)$$

or, for a spin-1/2 target

$$\mathcal{F}_{\mu\nu}(P,q) = q^2|F_1(q^2) + 2M_T F_2(q^2)|^2 \left(\delta_{\mu\nu} - \frac{q_\mu q_\nu}{q^2}\right) + \left(|F_1(q^2)|^2 + q^2|F_2(q^2)|^2\right) 4 \left(P_\mu - \frac{1}{2}q_\mu\right)\left(P_\nu - \frac{1}{2}q_\nu\right) \tag{6}$$

where a standard dipole fit was used for calculations

$$f_{1p} = f_{2p} = f_{2n} = \frac{1}{(1 + 1.21q^2/M_p^2)^2}, \qquad f_{1n} = 0. \tag{7}$$

Total Cross Section

- We integrated the 4 particle final state as outlined by Czyz et al. [1].
- To overcome the fact that the differential cross section is extremely peaked, we implemented a change of variables suggested by Lovseth et al. [4].
- We used the VEGAS [17] algorithm through the CUBA [18] and GSL [19] libraries

Outline

Coherent Process The nuclear form factor strongly limits the cross section

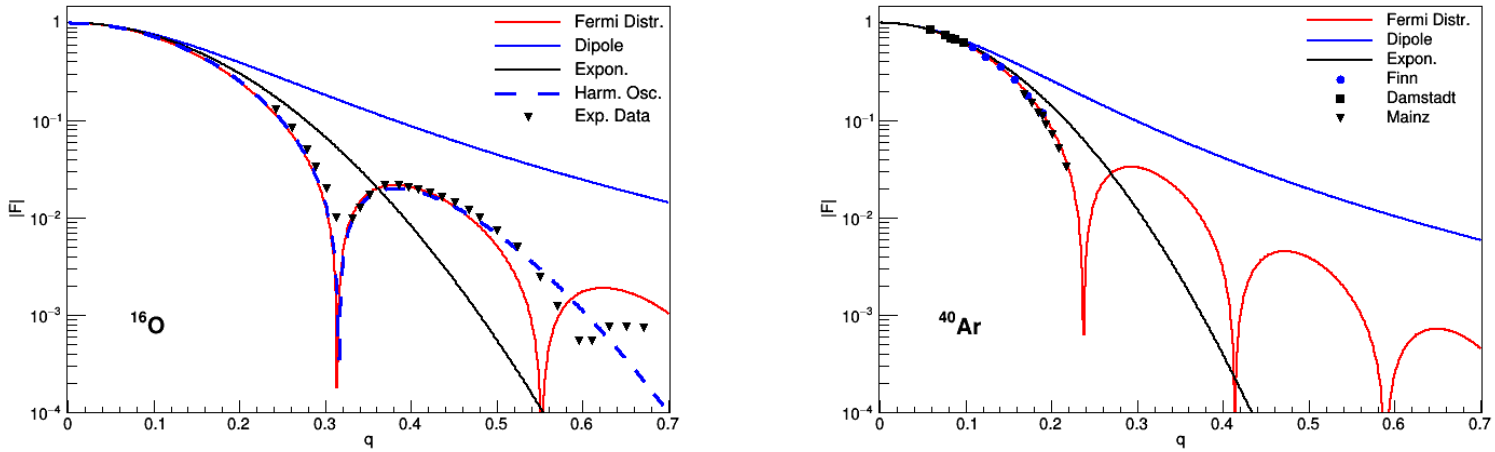

(a) O-16 (b) Ar-40

Figure: Comparison of different form factor models for relevant target nuclei. Measurement references are from [20].

Standard parameterizations are the dipole and exponential fit,

$$F(q^2) = \frac{1}{\left(1 - q^2 R_0^2/20\right)^2}, \qquad F(q^2) = e^{q^2 R_0^2/10}, \tag{8}$$

Outline

Incoherent Process

Nuclear physics strikes back hard here:

- at final state, Pauli blocking
- at initial state, nucleon Fermi momentum
- and we are neglecting many-body correlations among nucleons...

Assuming an ideal Fermi gas, we approximate the first effect with [4]

$$d\sigma_{\text{tot}} = d\sigma_{\text{coh}} + X^{\text{excl}}(|\vec{q}|)\,[N d\sigma_{\text{n}} + Z, d\sigma_{\text{p}}] \tag{11}$$

$$\begin{aligned} X^{\text{excl}}(|\vec{q}|) &= \begin{cases} 1.5\left(\frac{|\vec{q}|}{2p_f}\right) - 0.5\left(\frac{|\vec{q}|}{2p_f}\right)^3, & |\vec{q}| < 2p_f \\ 1, & \text{otherwise} \end{cases} \\ , p_f &= 235\text{MeV/c} \end{aligned} \tag{12}$$

Outline

Full calculation

The full SM cross section has the structure

$$\sigma^{SM} = C_V^2 \sigma_{C_V^2} + C_A^2 \sigma_{C_A^2} + C_V C_A \sigma_{C_V C_A}$$

$$\sigma^{SM} = \frac{1}{2}\left(C_V^2 + C_A^2\right)\sigma^{V-A}, \tag{13}$$

which we verified by doing the full calculation from effective lagrangian

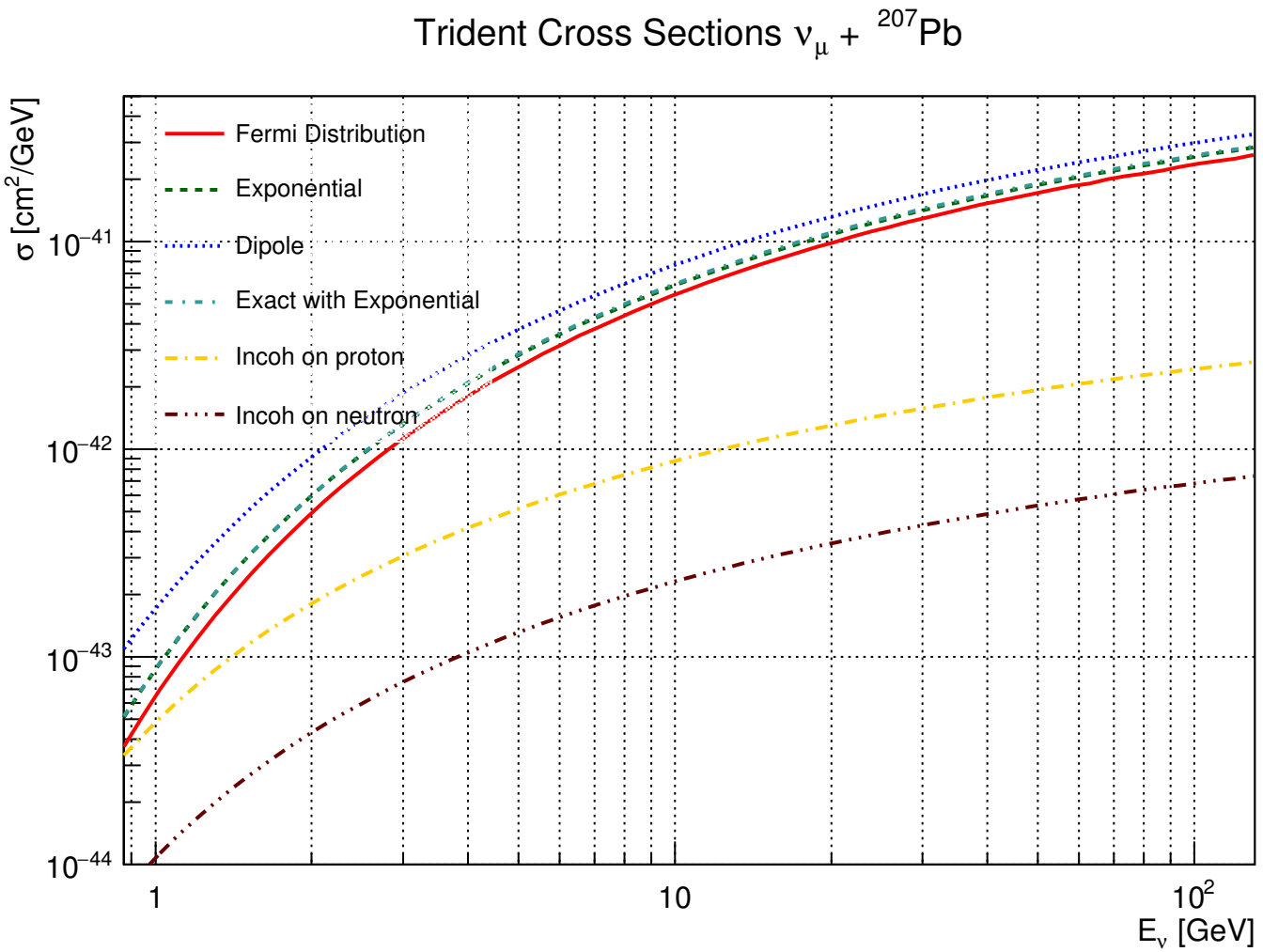

Figure: Total cross section for $\nu_\mu + {}^{207}Pb \to {}^{207}Pb + \mu^+ + \mu^- + \nu_\mu$ several nuclear form factors. Also shown the incoherent contributions per nucleus and exact calculation with exponential form factor.

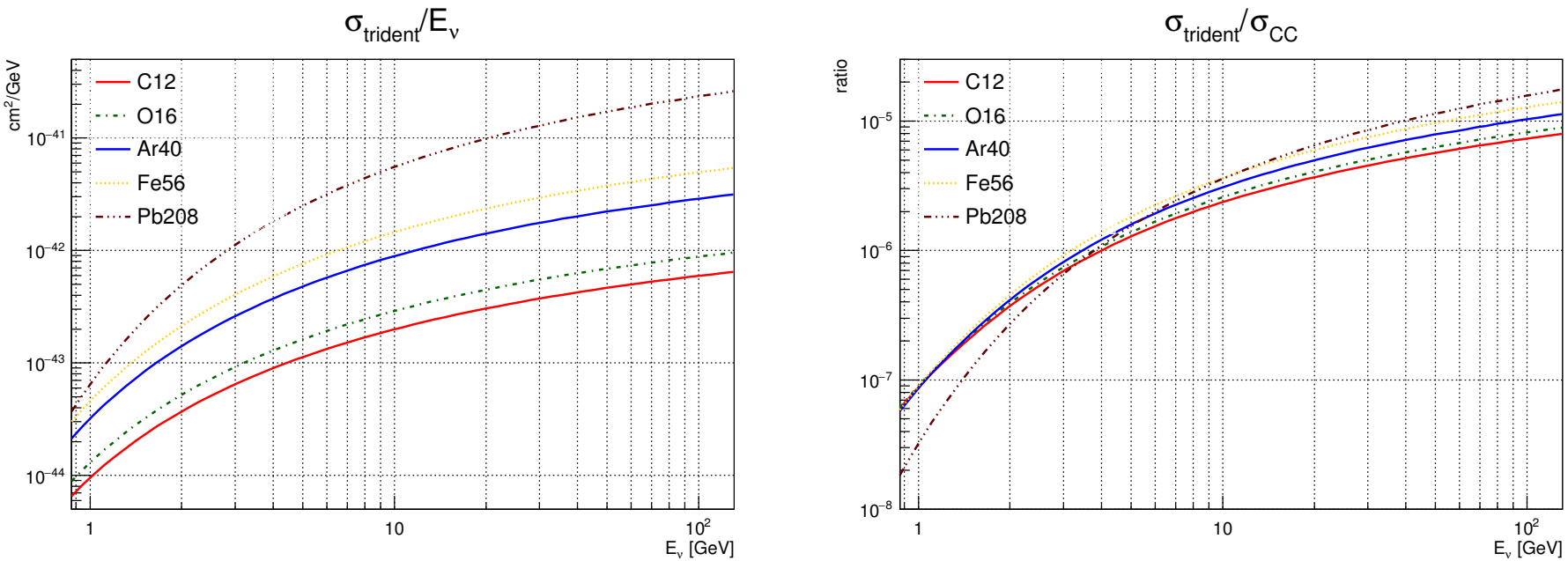

Figure: Comparison of total cross section for different Z to inclusive CC cross sections for different nuclei.

Simulation Framework

- We aim to improve separation of signal and background in non-oversimplified experimental setups
- We focus on accelerator-based neutrino experiments, given their high statistics and energy
- Representative of current experiments: NuMI flux in Medium Energy (ME) tune

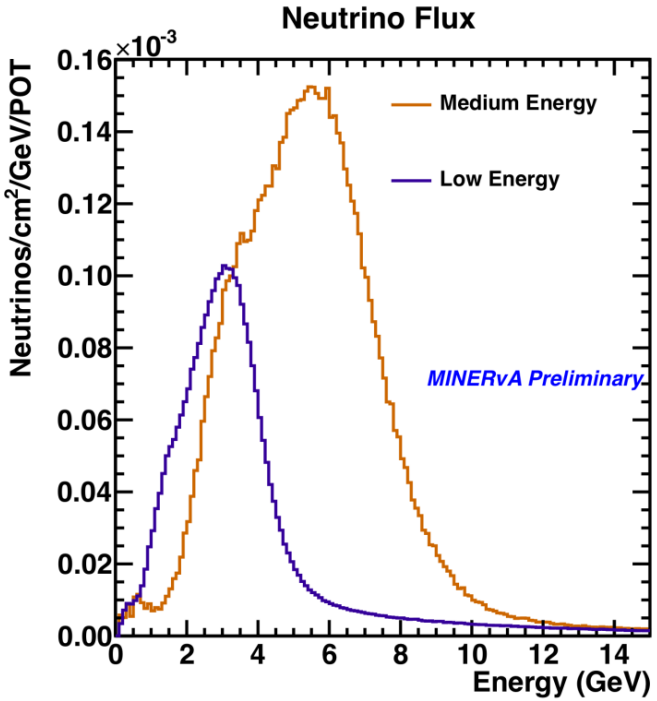

(a)

Figure: NuMI muon neutrino fluxes 9a) Low and Medium Energy tunes (from ref. [22])

Detector simulation:
MINERνA-like fine grained organic scintillator tracker, with GEANT4 v.10.3.1

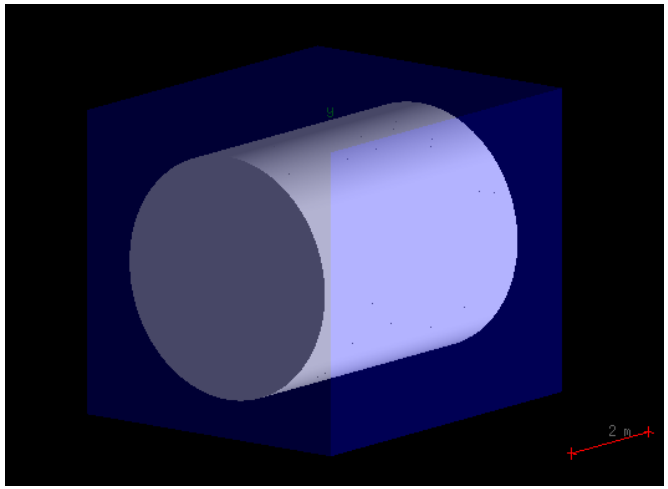

Interaction Simulation: GENIE v.2.12.4

- Signal: Custom new event generation thread
- Backgrounds: Default physics models in the MC

And finally, signal/background separation analysis using TMVA [23] v4.2.0 with both linear and non-linear methods

Outline

Signal Events

Experimental signature:

- two oppositely charged muon-like particles originating from the same vertex
- hadronic visible energy consistent with zero is required (form factor cuts off large q^2)
- very small muon-like pair invarinant mass [3]

Furhter details of our custom trident implementation are to be found elsewhere [24]

Outline

Backgrounds

Charm CC production

$$\nu_\mu + s/d \rightarrow \mu^{\mp} + c$$

$$c \rightarrow s/d + \mu^{\pm} + \nu_\mu$$

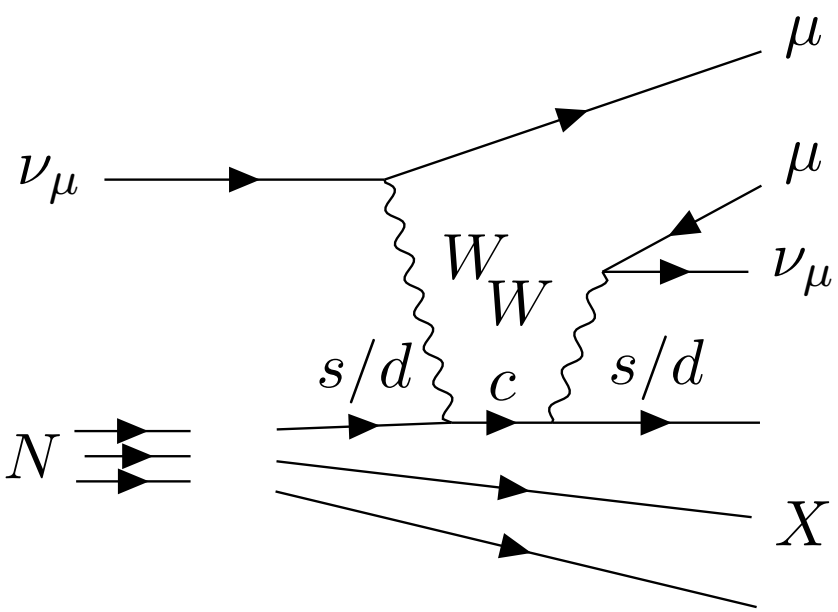

- Generally associated with a hadronic cascade near the vertex, which automatically discards it
- Charmed resonance excitations, e.g. Λ_c^+ decay very quickly and occur in more quasielastic-like events, thus we simulate and examine this background

Inclusive single charged pion production

$$\nu_\mu + N \rightarrow \mu^\mp + X + \pi^\pm$$
$$\pi^\pm \rightarrow \mu^\pm + \nu_\mu$$

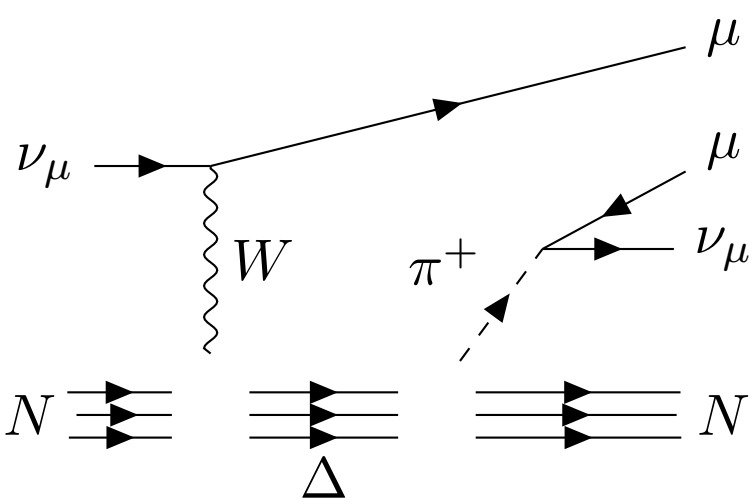

- Can yield dimuon-like events after complex convolution of interaction channel and Final State Interactions
- Events having either
  - passing pions, i.e escaping the detector
  - small angle pions, i.e. pions decaying very forwwardly (< 0.5) into antimuons

  are backgrounds to analyze
- Physics Models include indirect pion production (e.g. DIS) and direct pion production (e.g. Berger-Sehgal Coherent [25], Rein Diffractive [26])

Other sources

NC diffractive J/ψ production and decay to $\mu^+\mu^-$ was excluded in the CCFR [27] analysis removing invariant mass around J/ψ peak, 3.1 ± 0.4 GeV

We don't consider this background as the invariant mass distribution for trident is already strongly suppressed beyond 1 GeV

Analysis Methods

We aim to extract as much of the remaining information possible from kinematics, through six observables:

Observable	Description	Reconstruction Requirements
Z_{int}	Longitudinal position of interaction vertex	Vertexing
θ_+	Track polar angle of positive particle (w.r.t. beam axis)	Tracking, charge ID
θ_-	Track polar angle of negative particle (w.r.t. beam axis)	Tracking, charge ID
θ_{+-}	Angular separation between positive and negative particle tracks	Tracking
E_{+-}	Energy difference between positive and negative particles	Muon calorimetry (charge ID for sign)
W_{+-}	Invariant mass of positive and negative particles	Full muon momentum

Then we explore MVA techniques with both linear and non-linear methods. We finally report:

- Boosted Fisher (BF): base linear method optimizes separation with hyperplane in phase space. It is non-linearized through *boosting* (Adaptive Boost [23]).
- Boosted Decision Trees (BDT): generalizes rectangular cuts to subregions of the phase space, relies on boosting to avoid overtraining

To encompass variations in detector capabilities and/or reconstruction possilities within subregions in a detector, we examine five scenarios of variable availability

Scenario	Available observables						# of vars
1		θ_+	θ_-	θ_{+-}	E_{+-}	W_{+-}	5
2		θ_+	θ_-	θ_{+-}	E_{+-}		4
3	Z_{int}	θ_+	θ_-	θ_{+-}			4
4	Z_{int}	θ_+	θ_-				3
5	Z_{int}	θ_+					2
6				θ_{+-}	$\lvert E_{+-}\rvert$	W_{+-}	3
7				θ_{+-}	$\lvert E_{+-}\rvert$		2
8	Z_{int}			θ_{+-}			2
9		θ_+	θ_-	θ_{+-}			3
10		θ_+	θ_-				2

Removal order first driven by reconstruction requirements, then by classification power and correlations in exploratory analysis

- For each scenario, the full training, testing and evalutaion cycle of TMVA was run
- Passing pions are excluded in scenarios with muon calorimetry implied
- Scenarios account for charge ID availability (1-5, vs 6-8) and the pure angluar case (9-10)
- Enough events were generated of signal and background to train the methods

Results

Input variables (no passing pions included)

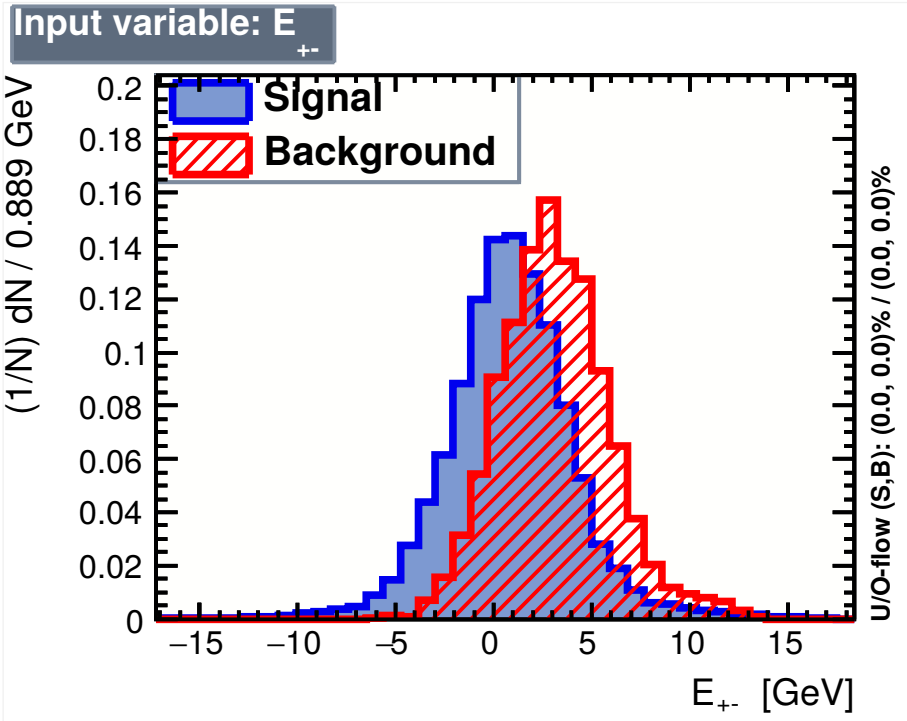

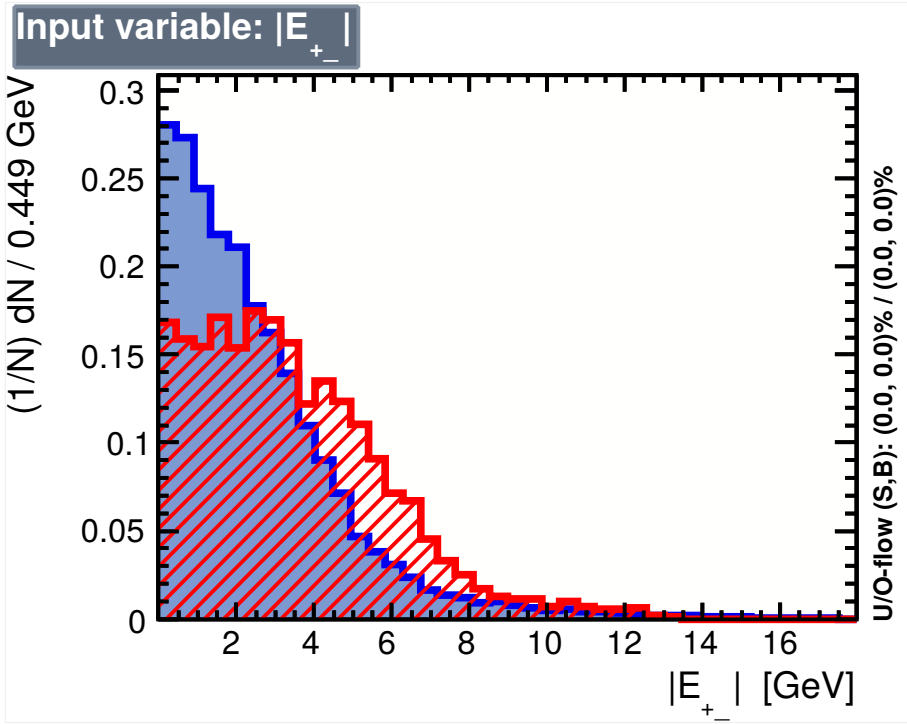

Input variables (no passing pions included)

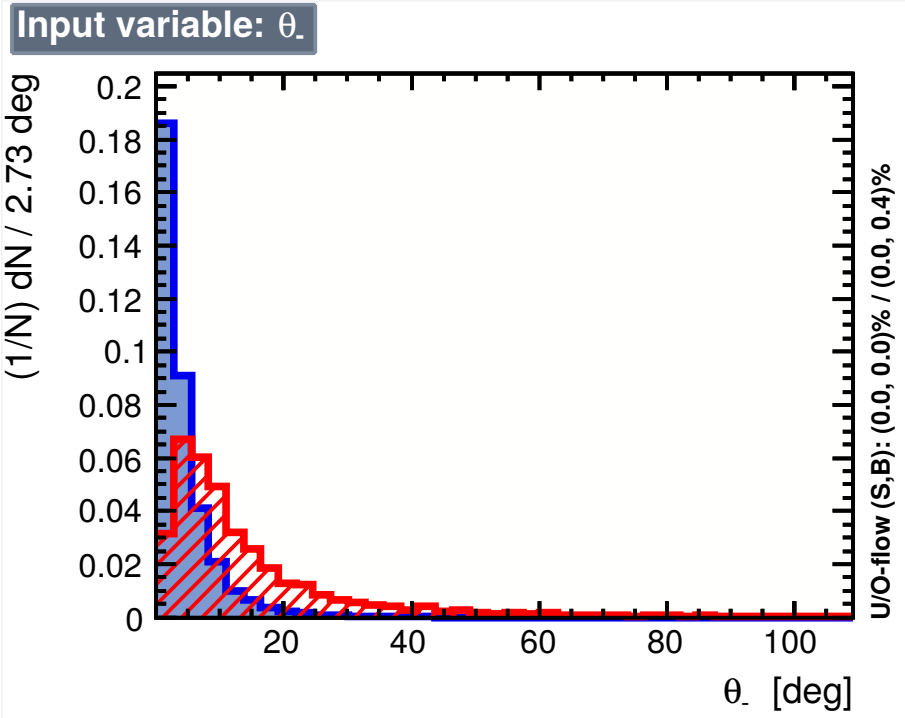

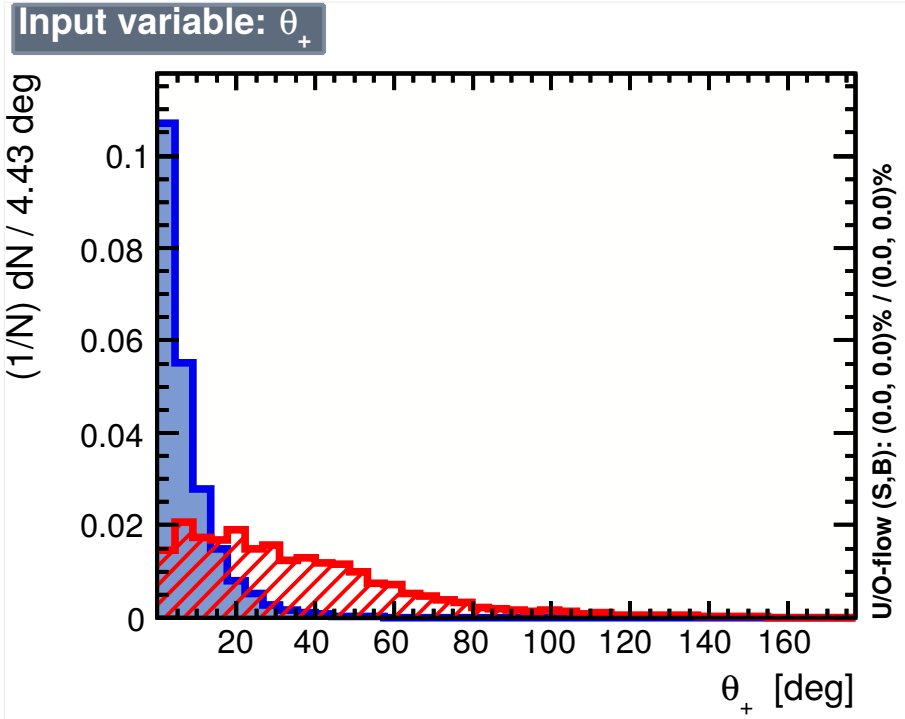

Input variables (no passing pions included)

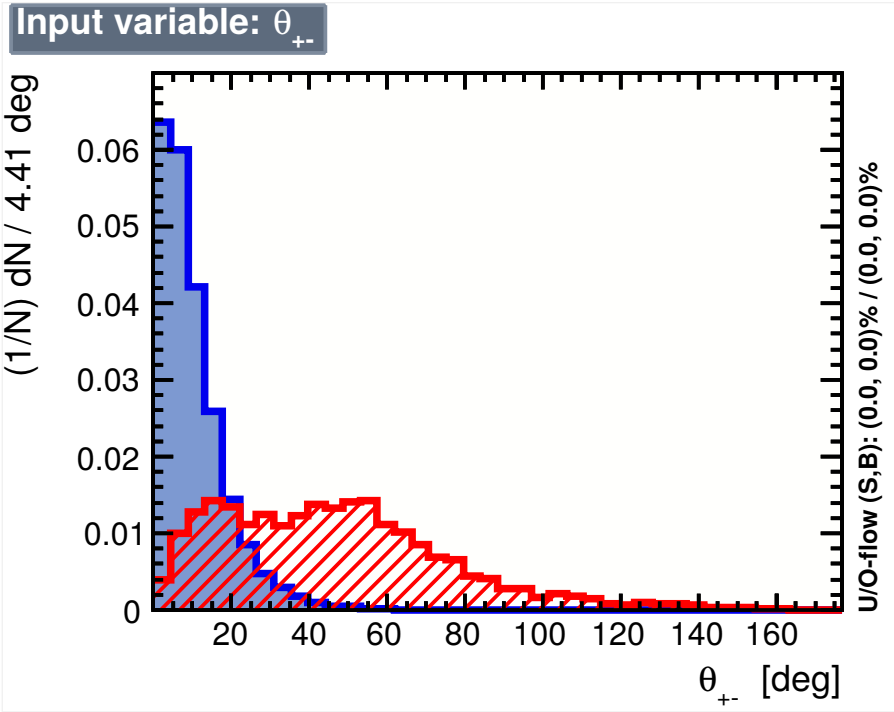

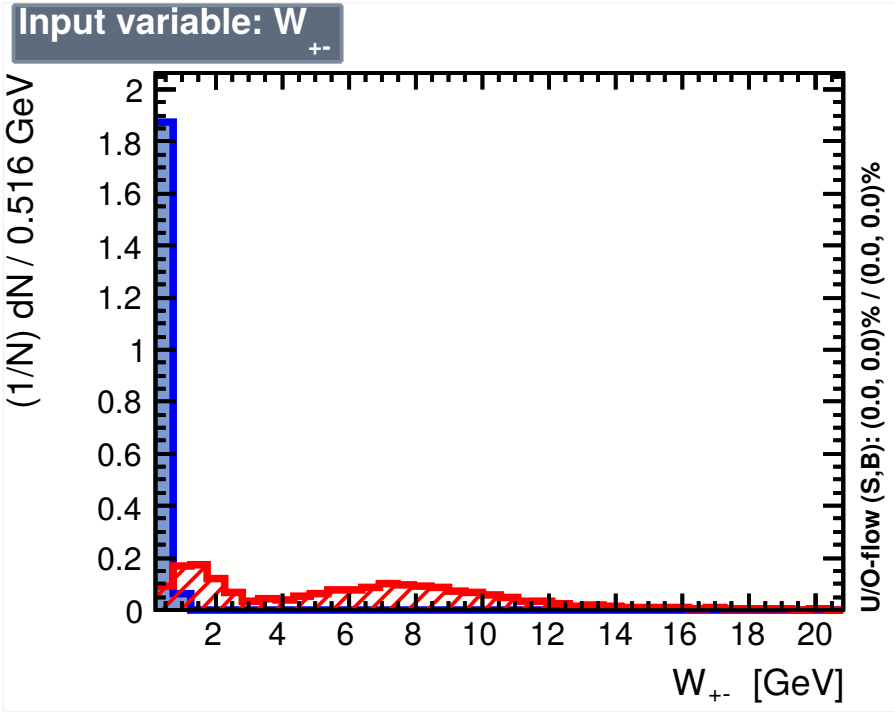

Input variables (with passing pions included)

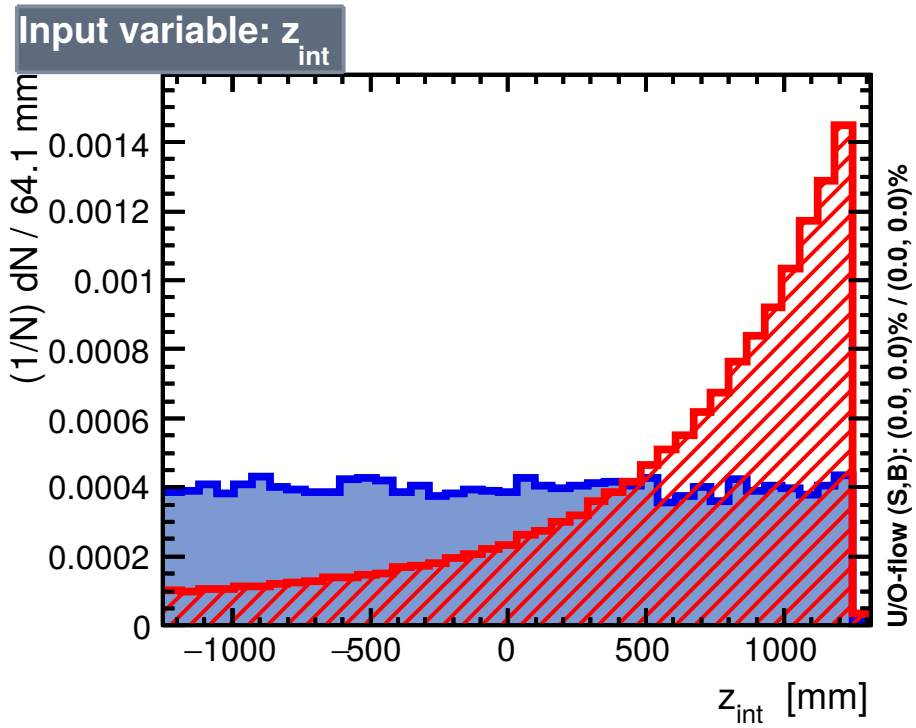

General comments

- Invariant mass seems to have the greatest separation power, followed by $_+$ and θ_-
- Recall muons are more symmetric for trident than for background
- $Z_{in}t$ is not outstanding, but is always available
- More information is expected in θ_+ and θ_- than with θ_{+-} alone

Global method comparison

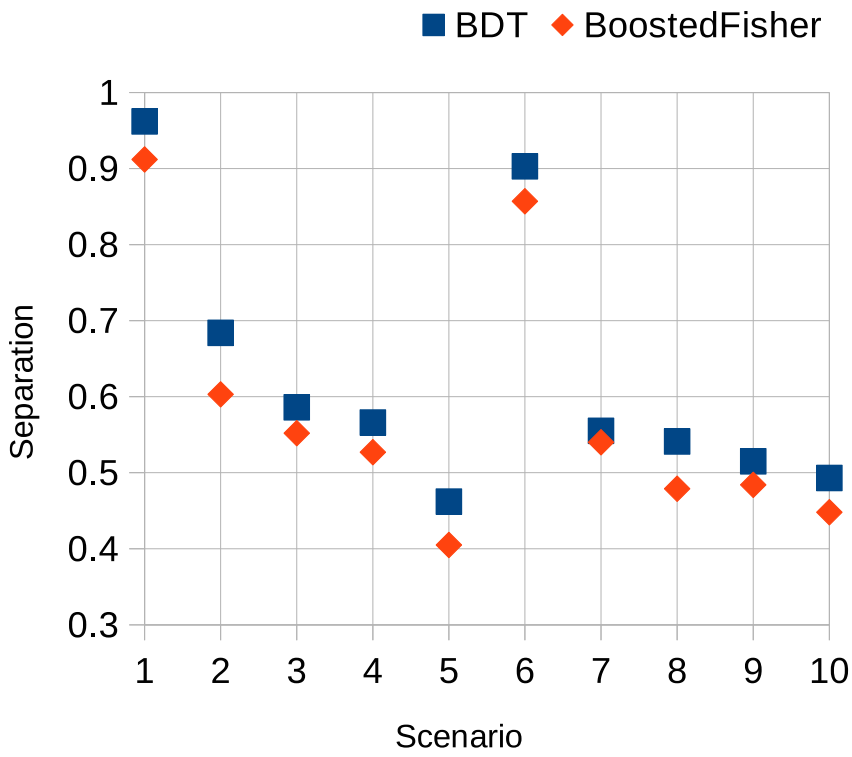

(a) Separation

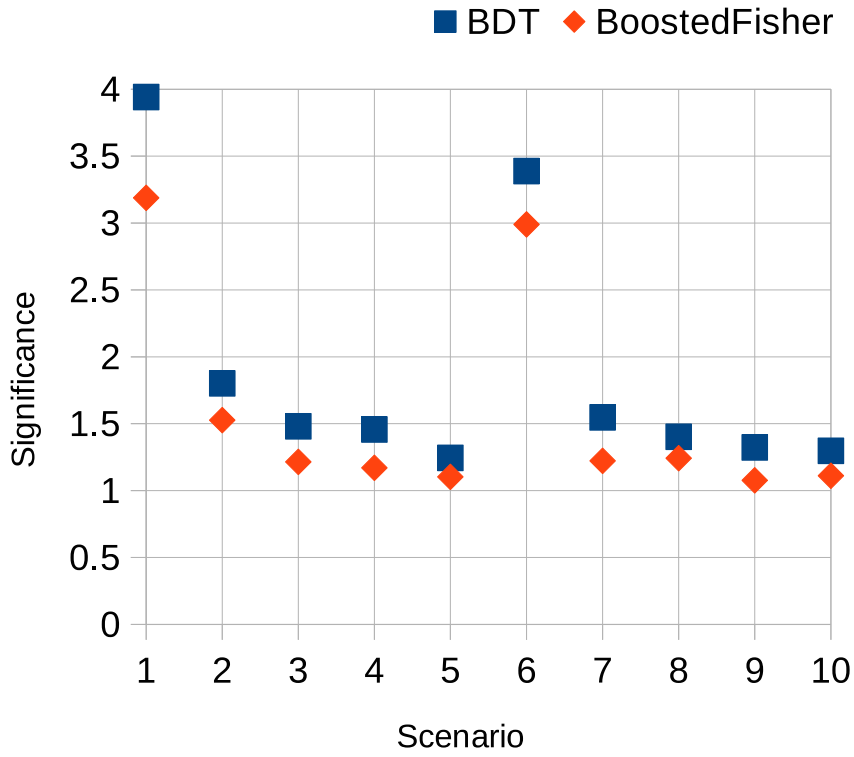

(b) Significance

- Notorious decrease in performance when W_{+-} and then θ_{-} are removed
- Noteworthy how boosting improved Fisher discriminant
- Both of the selected methods are very fast to train and apply, and also somehow transparent
- We also include checks for overtraining and proper forest development for BDT

Overtraining and cut values

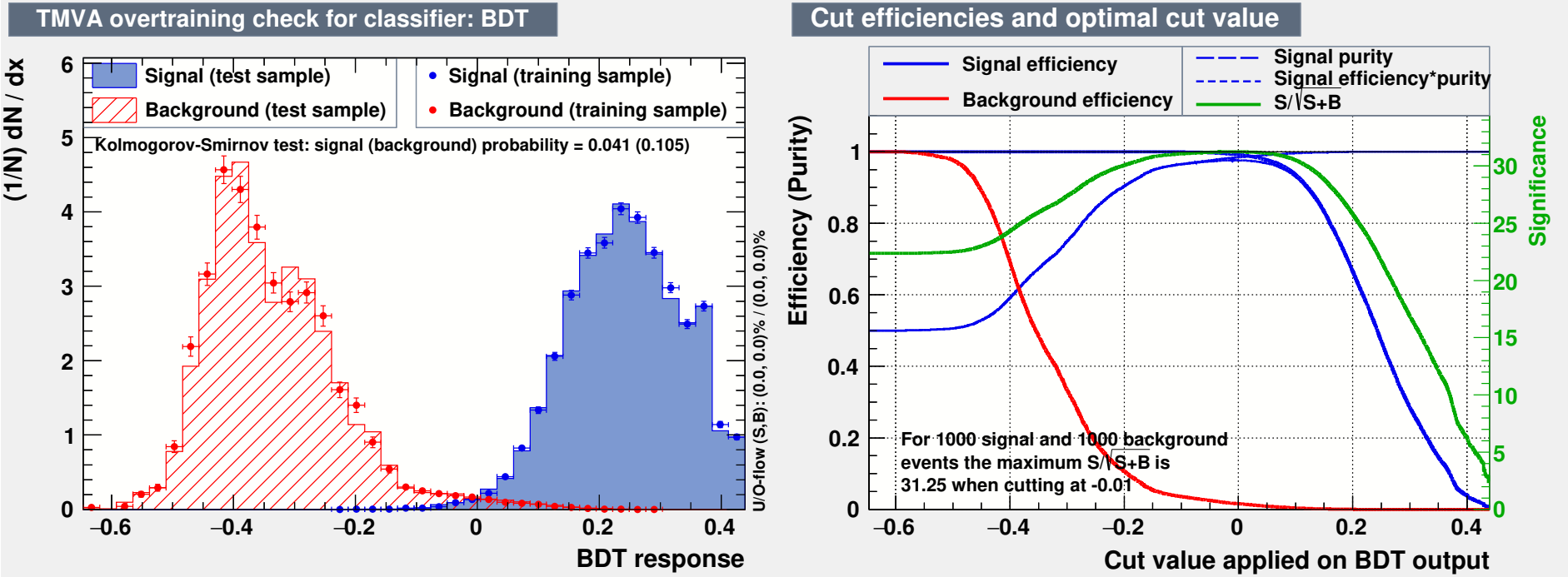

Figure: BDT Classifier

Overtraining and cut values

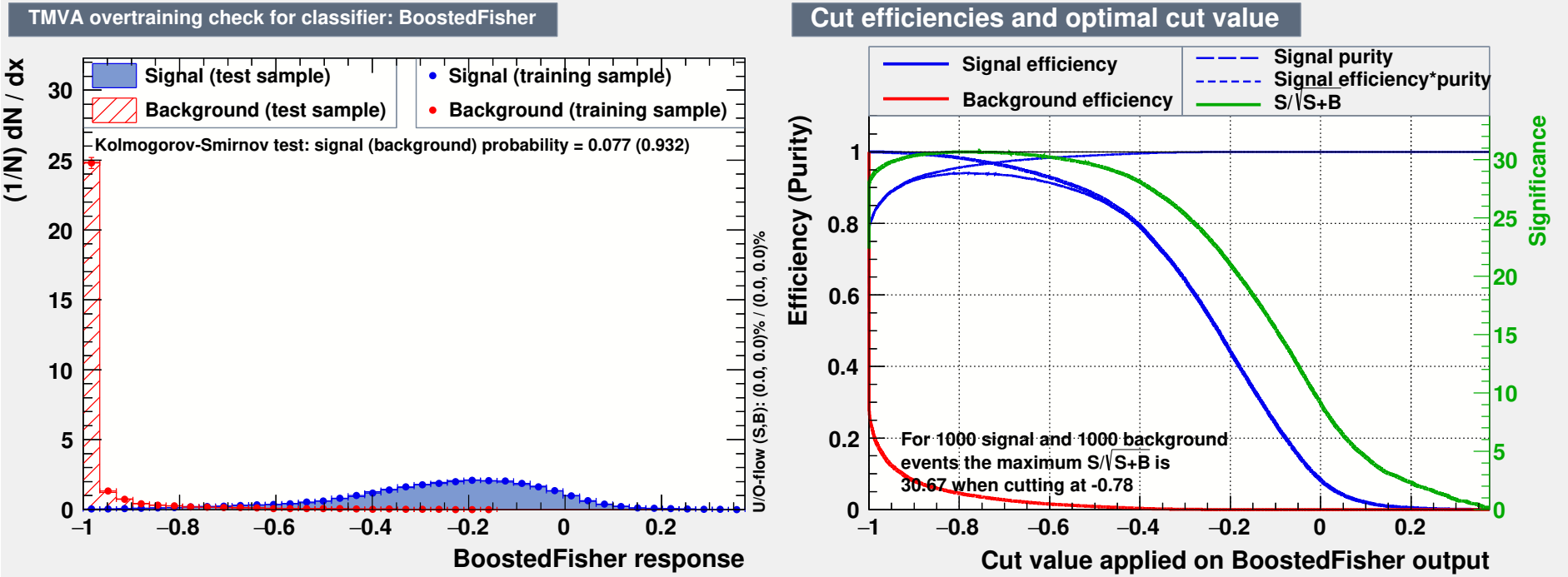

Figure: Boosted Fisher Classifier

Conclusions

- We have implemented a detailed simulation of neutrino trident production and reanalyzed relevant backgrounds with the GENIE and GEANT4 current framework
- We chose the NuMI ν_μ flux in Medium Energy tune and a detector simulation mimicking at some level a fine grained tracker like MINERνAor an option for the DUNE Near Detector
- We optimized signature selection with BDT multivariate analysis method in several scenarios
- We find that the invariant mass has the greatest separation power, reaching up to 4σ when all observables are available

BACKUP

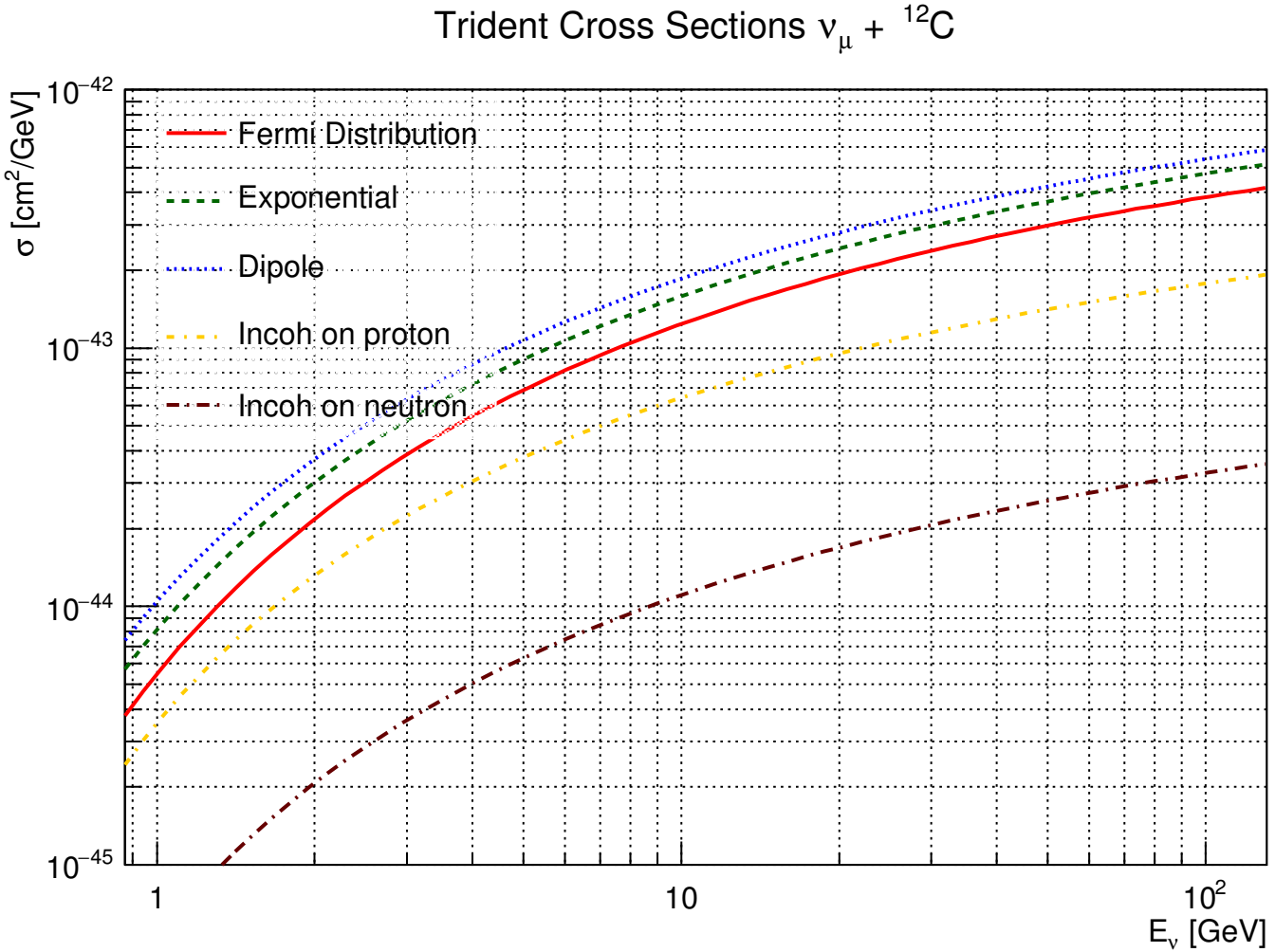
Trident Cross Sections ν_μ + ^{12}C
σ [cm^2/GeV]
10^{-42}
10^{-43}
10^{-44}
10^{-45}
Fermi Distribution
Exponential
Dipole
Incoh on proton
Incoh on neutron
1
10
10^2
E_ν [GeV]

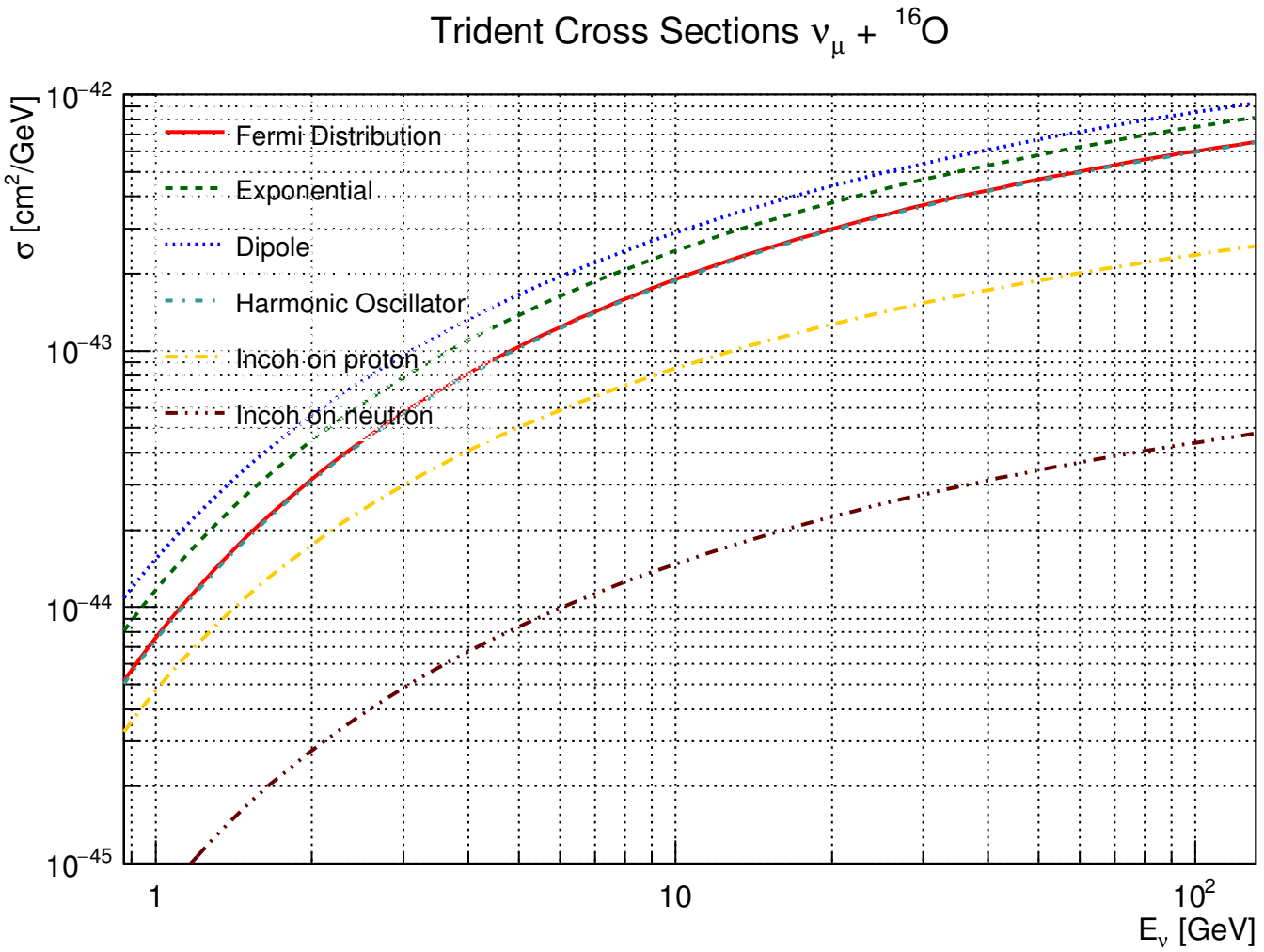
Trident Cross Sections ν_μ + ^{16}O
σ [cm^2/GeV]
10^{-42}
10^{-43}
10^{-44}
10^{-45}
Fermi Distribution
Exponential
Dipole
Harmonic Oscillator
Incoh on proton
Incoh on neutron
1
10
10^2
E_ν [GeV]

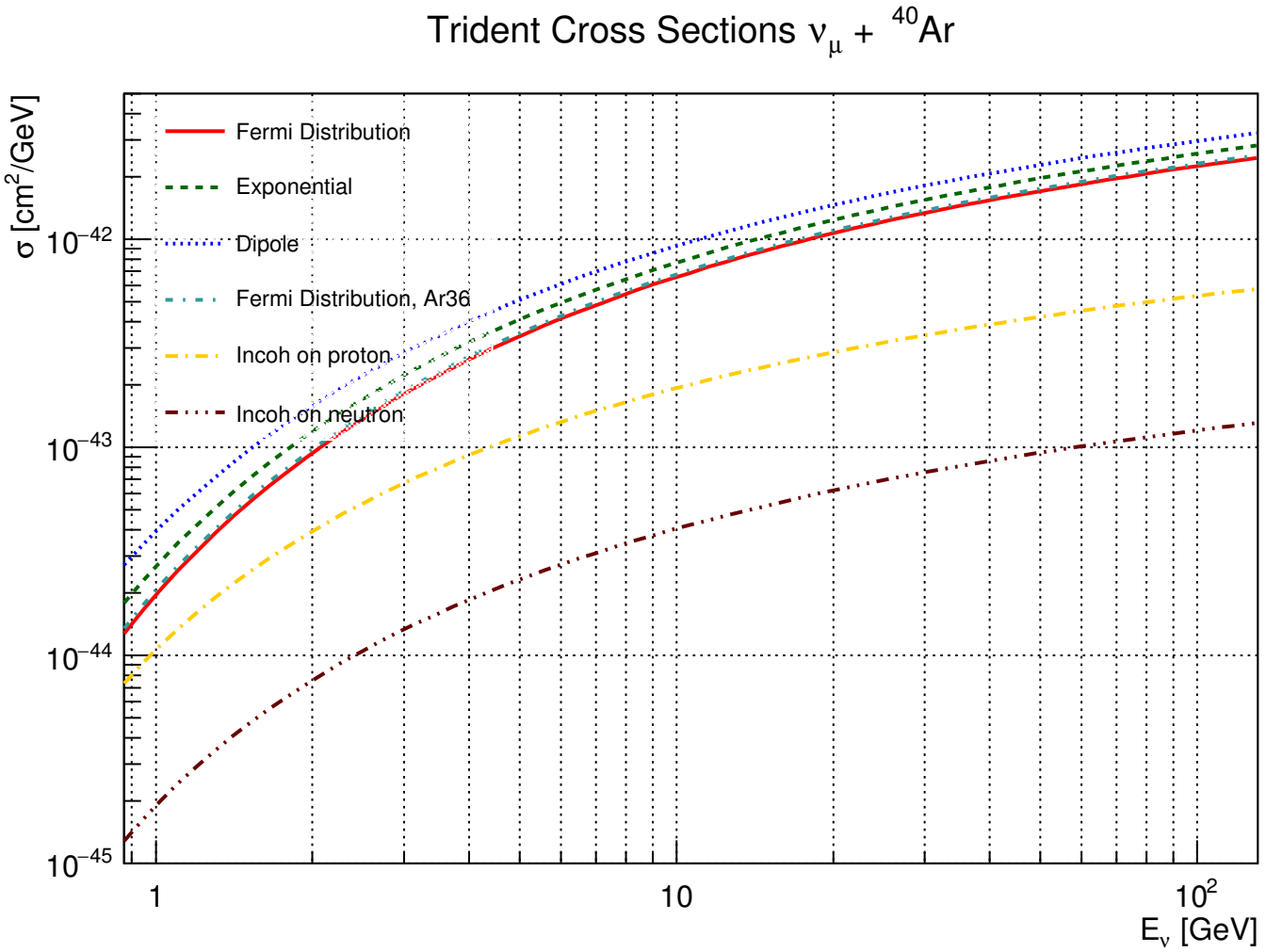
Trident Cross Sections ν_μ + ^{40}Ar
Fermi Distribution
Exponential
Dipole
Fermi Distribution, Ar36
Incoh on proton
Incoh on neutron
σ [cm^2/GeV]
10^{-42}
10^{-43}
10^{-44}
10^{-45}
1
10
10^2
E_ν [GeV]

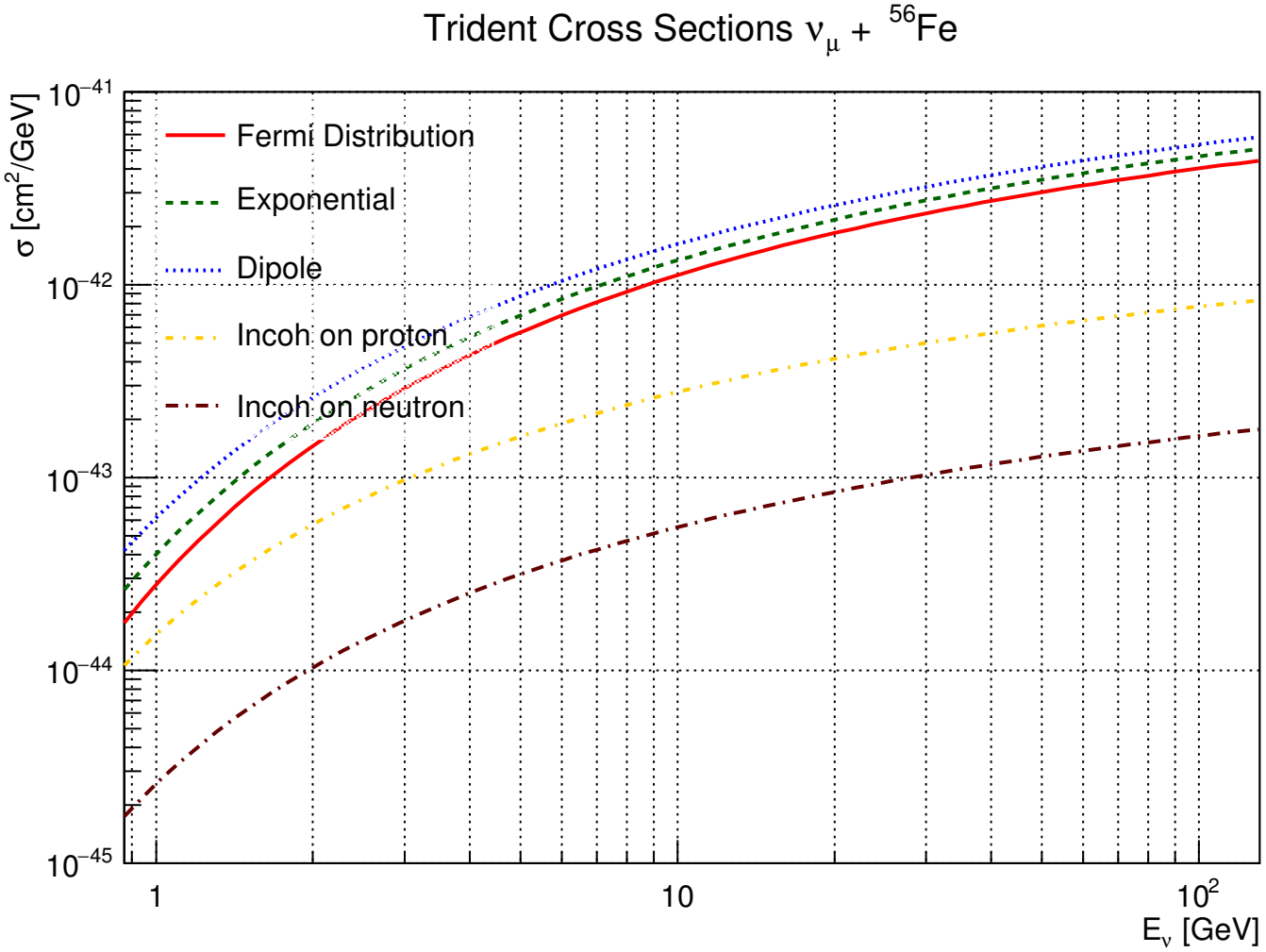
Trident Cross Sections ν_μ + ^{56}Fe
σ [cm^2/GeV]
10^{-41}
10^{-42}
10^{-43}
10^{-44}
10^{-45}
Fermi Distribution
Exponential
Dipole
Incoh on proton
Incoh on neutron
1
10
10^2
E_ν [GeV]

References


W. Czyz, G. C. Sheppey, and J. D. Walecka.
Neutrino production of lepton pairs through the point four-fermion interaction.
Nuovo Cim., 34:404–435, 1964.


M.S. Marinov, P. Nikitin, Y. P. Orevkov, and E. P. Shabalin.
Direct production of lepton pairs by a neutrino beam in the electromagnetic field of a nucleus.
Sov. J. Nucl. Phys, 3:497–503, 1966.


K. Fujikawa.
The self-coupling of weak lepton currents in high-energy neutrino and muon reactions.
Annals Phys., 68:102–162, 1971.


J. Lovseth and M. Radomiski.
Kinematical distributions of neutrino-produced lepton triplets.
Phys. Rev., D3:2686–2706, 1971.


R. W. Brown, R. H. Hobbs, J. Smith, and N. Stanko.
Intermediate boson. iii. virtual-boson effects in neutrino trident production.
Phys. Rev., D6:3273–3292, 1972.


R. Belusevic and J. Smith.
W - Z Interference in Neutrino - Nucleus Scattering.
Phys. Rev., D37:2419, 1988.


F. Bergsma et al.
Search for Coherent Muon Pair Production by Neutrinos and Anti-neutrinos.
Phys. Lett., B122:185, 1983.

D. Geiregat et al.
First observation of neutrino trident production.
Phys. Lett., B245:271–275, 1990.

B. A. Schumm et al.
Search for neutrino trilepton production in the Fermilab Tevatron neutrino beam by the CCFR Collaboration.
In *'88 electroweak interactions and unified theories. Proceedings, 23rd Rencontres de Moriond, Leptonic Session, Les Arcs, France, March 6-13, 1988*, pages 413–420, 1988.

Wolfgang Altmannshofer, Stefania Gori, Maxim Pospelov, and Itay Yavin.
Neutrino Trident Production: A Powerful Probe of New Physics with Neutrino Beams.
Phys. Rev. Lett., 113:091801, 2014.

P. Adamson et al.
The NuMI Neutrino Beam.
Nucl. Instrum. Meth., A806:279–306, 2016.

J. Nelson.
Neutrino-nucleus scattering results from MINERvA, part 1.
In *18th International Workshop on Neutrino Factories and Future Neutrino Facilities Search (NuFact16) Quy Nhon, Vietnam, August 21-27, 2016*, 2016.

L. Aliaga et al.
Design, Calibration, and Performance of the MINERvA Detector.
Nucl. Instrum. Meth., A743:130–159, 2014.

R. Acciarri et al.
Long-Baseline Neutrino Facility (LBNF) and Deep Underground Neutrino Experiment (DUNE).
2016.

Costas Andreopoulos, Christopher Barry, Steve Dytman, Hugh Gallagher, Tomasz Golan, Robert Hatcher, Gabriel Perdue, and Julia Yarba.
The GENIE Neutrino Monte Carlo Generator: Physics and User Manual.
2015.

S. Agostinelli et al.
GEANT4: A Simulation toolkit.
Nucl. Instrum. Meth., A506:250–303, 2003.

G. Peter Lepage.
A New Algorithm for Adaptive Multidimensional Integration.
J. Comput. Phys., 27:192, 1978.

T. Hahn.
CUBA: A Library for multidimensional numerical integration.
Comput. Phys. Commun., 168:78–95, 2005.

GSL Project Contributors.
GSL - GNU scientific library - GNU project - free software foundation (FSF).
http://www.gnu.org/software/gsl/, 2010.

H. De Vries, C. W. De Jager, and C. De Vries.
Nuclear charge and magnetization density distribution parameters from elastic electron scattering.
Atom. Data Nucl. Data Tabl., 36:495–536, 1987.

M. E. Grypeos, G. A. Lalazissis, S. E. Massen, and C. P. Panos.
The 'COSH' or symmetrized Woods-Saxon nuclear potential.
Submitted to: J. Phys. G, 1991.


Laura Fields.
Recent Results from MINERvA.
In *27th International Conference on Neutrino Physics and Astrophysics (Neutrino 2016) London, United Kingdom, July 4-9, 2016*, 2016.


Andreas Hoecker, Peter Speckmayer, Joerg Stelzer, Jan Therhaag, Eckhard von Toerne, and Helge Voss.
TMVA: Toolkit for Multivariate Data Analysis.
PoS, ACAT:040, 2007.


S.Sánchez Falero, E. Endress, J.Becerra, and A.M.Gago.
Implementation and validation of Neutrino Trident Production Processes in the GENIE Neutrino MC Generator.
In preparation.

Ch. Berger and L. M. Sehgal.
Partially conserved axial vector current and coherent pion production by low energy neutrinos.
Phys. Rev. D, 79:053003, Mar 2009.

D. Rein.
Diffractive Pion Production in Neutrino Reactions.
Nucl. Phys., B278:61–77, 1986.

S. R. Mishra et al.
Neutrino tridents and W Z interference.
Phys. Rev. Lett., 66:3117–3120, 1991.